



HAL
open science

Deciphering human-climate interactions in an ombrotrophic peat record: REE, Nd and Pb isotope signatures of dust supplies over the last 2500 years (Misten bog, Belgium)

Nathalie Fagel, Mohammed Allan, Gaël Le Roux, Nadine Mattielli, Natalia Piotrowska, Jaroslaw Sikorski

► **To cite this version:**

Nathalie Fagel, Mohammed Allan, Gaël Le Roux, Nadine Mattielli, Natalia Piotrowska, et al.. Deciphering human-climate interactions in an ombrotrophic peat record: REE, Nd and Pb isotope signatures of dust supplies over the last 2500 years (Misten bog, Belgium). *Geochimica et Cosmochimica Acta*, 2014, vol. 135, pp. 288-306. 10.1016/j.gca.2014.03.014 . hal-00988093

HAL Id: hal-00988093

<https://hal.science/hal-00988093>

Submitted on 7 May 2014

HAL is a multi-disciplinary open access archive for the deposit and dissemination of scientific research documents, whether they are published or not. The documents may come from teaching and research institutions in France or abroad, or from public or private research centers.

L'archive ouverte pluridisciplinaire **HAL**, est destinée au dépôt et à la diffusion de documents scientifiques de niveau recherche, publiés ou non, émanant des établissements d'enseignement et de recherche français ou étrangers, des laboratoires publics ou privés.



Open Archive TOULOUSE Archive Ouverte (OATAO)

OATAO is an open access repository that collects the work of Toulouse researchers and makes it freely available over the web where possible.

This is an author-deposited version published in : <http://oatao.univ-toulouse.fr/>
Eprints ID : 11538

To link to this article : DOI: 10.1016/j.gca.2014.03.014
<http://dx.doi.org/10.1016/j.gca.2014.03.014>

To cite this Fagel, Nathalie and Allan, Mohammed and Le Roux, Gaël and Mattielli, Nadine and Piotrowska, Natalia and Sikorski, Jaroslaw *Deciphering human–climate interactions in an ombrotrophic peat record: REE, Nd and Pb isotope signatures of dust supplies over the last 2500 years (Misten bog, Belgium)*. (2014) *Geochimica et Cosmochimica Acta*, vol. 135 . pp. 288-306. ISSN 0016-7037

Any correspondence concerning this service should be sent to the repository administrator: staff-oatao@listes-diff.inp-toulouse.fr

Deciphering human–climate interactions in an ombrotrophic peat record: REE, Nd and Pb isotope signatures of dust supplies over the last 2500 years (Misten bog, Belgium)

N. Fagel^{a,*}, M. Allan^a, G. Le Roux^b, N. Mattielli^c, N. Piotrowska^d,
J. Sikorski^d

^a *AGEs, Department of Geology, Université de Liège ULg, Belgium*

^b *EcoLab, ENSAT, Avenue de l'Agrobiopole, 31326 Castanet Tolosan, France*

^c *G-Time, Université Libre Bruxelles ULB, Brussels, Belgium*

^d *Department of Radioisotopes, GADAM Centre of Excellence, Institute of Physics, Silesian University of Technology, Gliwice, Poland*

Abstract

A high-resolution peat record from Eastern Belgium reveals the chronology of dust deposition for the last 2500 years. REE and lithogenic elements in addition to Nd and Pb isotopes were measured in a 173 cm age-dated peat profile and provide a continuous chronology of dust source and intensity. Calculated dust flux show pronounced increases c. 300 BC, 600 AD, 1000 AD, 1200 AD and from 1700 AD, corresponding to local and regional human activities combined with climate change.

The Industrial Revolution samples (1700–1950 AD) are characterised by a significant enrichment in Sc-normalised REE abundance (sum REE/Sc > 25) due to intensive coal combustion. For the pre-Industrial Revolution samples, the Sc-normalised REE abundance (10 < Sum REE/Sc < 25) and the ϵ Nd variability (–13 to –9) are interpreted by a mixing between dust particles from local soils and long-range transport of desert particles. Three periods characterised by dominant-distal sources (c. 320 AD, 1000 AD and 1700 AD) are consistent with local wetter-than-average intervals as indicated by a lower degree of peat humification. Local erosion prevails during the drier (higher humification) intervals (100 AD, 600 AD). On a global scale, more distal supplies are driven during colder periods, in particular during the Oort and Maunder minima, suggesting a potential link between dust deposition and global climate. Combining REE abundance, fractionation between Light REE and Heavy REE and Nd isotope data in ombrotrophic peat allows one to distinguish between dust flux changes related to human and climate forcings.

1. INTRODUCTION

Our knowledge of climate evolution is derived from the analysis of biological and geological archives, such as tree

rings (e.g., [Lieubeau et al., 2007](#)), ice cores (e.g., [Lambert et al., 2012](#)), marine and lacustrine sediments (e.g., [Bradley, 1999](#)). Peatlands (i.e., soils accumulating partially decomposed plant remains with above 50% of organic matter and greater than 30 cm deep, [Clymo, 1987](#)) are continental archives of particular interest because they are easy to date, have a high temporal resolution (decadal) and contain multiple measurable parameters dependent on environmental conditions including temperature and/or humidity,

* Corresponding author. Tel./fax: +32 4 3662029.

E-mail addresses: nathalie.fagel@ulg.ac.be (N. Fagel), gael.leroux@ensat.fr (G. Le Roux), nmattiel@ulb.ac.be (N. Mattielli), natalia.piotrowska@polsl.pl (N. Piotrowska).

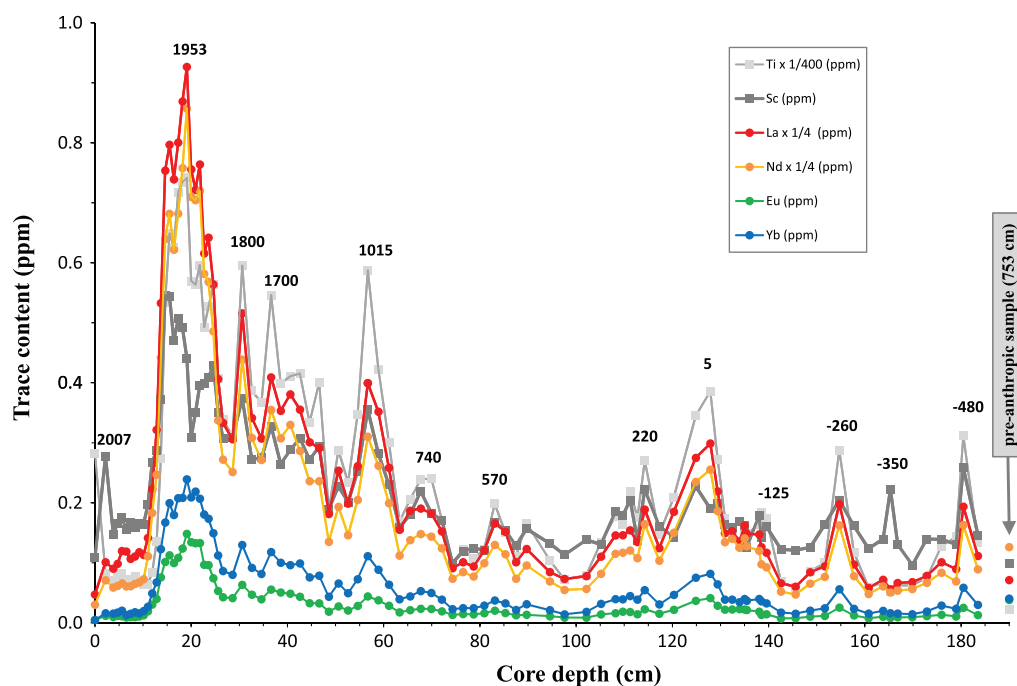


Fig. 1. Profile of REE and Sc, Ti content (in ppm) vs. core depth (in cm). We report La and Nd as LREE, Eu and Gd as MREE and Yb and Lu as HREE. The REE vary in parallel with the lithogenic elements such as Sc or Ti. The pre-anthropogenic values measured at the base of the peat profile (753 cm, 7500 BP) are plotted for comparison. The numbers give an indication about the age in years (positive values for AD, negative values for BC). Data from Table 1.

atmospheric circulation and wind strength (e.g., Chambers et al., 2012). In particular ombrotrophic bogs are commonly used to reconstruct Holocene climate variability (e.g., Dupont, 1986; Hong et al., 2000; Shotyk et al., 2002; Mauquoy et al., 2002; Chambers and Charman, 2004; Roos-Barraclough et al., 2004; Sapkota et al., 2007; Lamentowicz et al., 2008; Moschen et al., 2011; Kylander et al., 2013). Ombrotrophic environments are hydrologically isolated from the surrounding landscapes; they receive all of their water and nutrients from precipitation (rain, snow, fog) and wind, with no influence from streams (e.g. Chambers and Charman, 2004). Ombrotrophic peatland is often bog, dominated by *Sphagnum* mosses. In comparison with ice cores, they have two main advantages: (1) a widespread terrestrial global distribution, providing easy access and sampling, (2) the easy application of radioisotope dating techniques (^{210}Pb and ^{14}C). Since ombrotrophic peat is almost exclusively constituted of organic matter, it yields high-resolution and low-uncertainty chronologies (Charman and Mäkilä, 2003).

In addition to pollen (e.g. Persch, 1950; Anshari et al., 2001; Davis et al., 2003; Finsinger et al., 2006), there are a variety of complementary potential indicators of past climate in peatland profiles. Moisture content of the *Sphagnum* mosses, water table depth, humification levels, macroremains and testate amoebae are directly linked to climate, and more specifically to the balance between evaporation and precipitation (e.g. McCarthy et al., 1995; Mauquoy et al., 2002; Barber et al., 2003; Roos-Barraclough et al., 2004; Lamentowicz et al., 2008;

Mitchell et al., 2008). The oxygen, carbon and deuterium stable isotope compositions of peat plant cellulose have been used to reconstruct air temperatures (Dupont, 1986; Hong et al., 2000; Moschen et al., 2011). Besides those classical biological proxies, the inorganic fraction of peat also provides information on the abundance and origin of atmospheric mineral dust affecting the Earth's climate system (Goudie and Middleton, 2001; Harrison et al., 2001; Oppenheimer, 2003).

North African deserts currently represent the largest worldwide source of mineral dust (Moulin et al., 1997), supplying $\sim 0.8 \times 10^9$ tons per year of material transported in suspension in the atmosphere (Goudie and Middleton, 2001; Laurent et al., 2008). According to Vanderstraeten et al. (2008), "the amount of airborne dust varies in accordance with the general and local meteorological situation, the complexity of relief forms, lithology and provenance (direction and distance from the source) of the dust". Dust is first uplifted by local winds, transported by an increased vertical velocity to higher latitudes (Engelstaedter and Washington, 2007) and then transported over hundreds to thousands of kilometers along three main transport pathways (Goudie and Middleton, 2001) (see SM1). Most of the dust is carried westward over the North Atlantic Ocean by the trade winds (D'Almeida, 1986; Kellogg and Griffin, 2006; Scheuven et al., 2013). However, due to peculiar meteorological conditions (e.g., low pressure systems, creation of easterly waves – White et al., 2012; Scheuven et al., 2013), an eastward or a northward flow may punctually bring dust across the Mediterranean Sea to adjacent

countries. Occasionally dust is even deposited north of the Alps, transported by anticyclonic cells and washed out by rain (see [Stuut et al., 2009](#) for a review). [White et al. \(2012\)](#) have reported more than 500 dust-fall events across Europe since 1900. For instance, in Belgium calculated backward trajectories have allowed the determination of a Saharan origin for a dust event observed in March 2007 above Brussels ([Vanderstraeten et al., 2008](#)).

Previous work has used peat cores as dust archives ([Shotyk et al., 1998, 2002](#); [Björck and Clemmensen, 2004](#); [Martini and Martinez-Cortizas, 2006](#); [Sapkota et al., 2007](#); [De Vleeschouwer et al., 2009](#); [Le Roux et al., 2012](#); [Kylander et al., 2013](#)). For instance [Shotyk et al. \(1998\)](#) used the geochemical signature of peat to reconstruct the atmospheric particulate flux for the entire Holocene in a 6 m bog in the Swiss Jura. The changes in dust flux were further linked to major modification in atmospheric trajectories and therefore to climate reorganisation. Later [Sapkota et al. \(2007\)](#) published a record of 6000 years of atmospheric dust deposition in southern South America and [Kylander et al. \(2013\)](#) have reconstructed 8500 years of dust deposition in Sweden.

Recently Nd isotope data from the same Swiss Jura bog confirmed the importance of Sahara desert as a dust source over West Europe ([Le Roux et al., 2012](#)). In particular a sharp dust event at 8.4 kyr may suggest a role of atmospheric dust in the inception of the 8.2 kyr BP cold event. Moreover a long-term change in Saharan-dust supplies evidenced from 7 to 5 kyr B.P is consistent with the termination of the African humid period (Sahara aridification). Such studies underline the importance of high-resolution peat bog investigations for a better understanding of the role of dust in Holocene climate change. However ombrotrophic bogs record both natural and anthropogenic dust supplies. For instance, based on a high resolution study on the Misten peatland [De Vleeschouwer et al. \(2012\)](#) emphasized that variations in dust fluxes, derived from the elementary composition of the upper first meter of peat, could not be directly interpreted in term of climate changes for the late Holocene, and especially for the past millennium, where both influences are difficult to distinguish. Therefore before making any climate interpretations, the sources of dust must be identified. Radiogenic isotope signatures of sediments are often used as provenance proxies as they are not affected by erosion and transport (i.e., conservative behavior during the sedimentary cycle, [Goldstein et al., 1984](#)). Pb isotopes, particularly in peatlands, have been often used as evidence of anthropogenic heavy metal pollution (e.g., [Shotyk et al., 1998](#); [Dunlap et al., 1999](#); [Klaminder et al., 2003, 2005](#); [Ferrat et al., 2012a,b](#)). Another radiogenic isotope system, the Sm/Nd, is less sensitive to trace metal pollution, but Nd isotope data for peat samples are scarce, and have only been measured at a few sites (Blue Cypress in Florida; [Kamenov et al., 2009](#); Etang de la Gruère in Switzerland, [Le Roux et al., 2012](#)). If their conservative behaviour can be demonstrated, both Nd and Pb isotopes may be used to discriminate between sources of dust in bogs.

In this study, we aim to measure REE content in peat samples to record the dust fluxes over the past 2500 years

in western Europe. We use their Nd isotope signatures to decipher between local and distal dust supplies, while Pb isotopes are used to trace anthropogenic influences. We interpret the changes in dust sources with regard to local hydrological conditions derived from humification degree (dry/wet) and global climate conditions (cold/warm) from solar activities.

2. MATERIAL AND METHODS

The present study is focused on the upper section of an ombrotrophic bog located in a nationally protected peatland area, the Hautes-Fagnes Plateau in East Belgium (~3750 ha, [Frankard et al., 1998](#)). The Hautes-Fagnes Plateau is part of the Stavelot Massif, mainly composed of lower Paleozoic quartzites and pyllades ([Verniers et al., 2001](#)). The geological substratum is covered by post-Paleozoic sediments (clays of alteration, continental and marine sands, loess – [Bourignon, 1953](#)) with some occasional outcrops of Early Cambrian (Revinian) quartzites. In the last 10 years, some geochemical work has been carried out on selected sites from the Hautes Fagnes Plateau ([Gaida et al., 1993, 1997](#); [Kempter, 1996](#); [Renson et al., 2008](#)) and in the Misten in particular ([De Vleeschouwer et al., 2007, 2009, 2010, 2012](#); [Allan et al., 2013a](#)). The selected Misten bog is produced by an accumulation of 8 m (estimated by a radar surface prospecting – [Wastiaux and Schumacker, 2003](#)) of Holocene peat ([De Vleeschouwer et al., 2007](#)). For this study, cores were taken in February 2008: the upper meter was retrieved with a Ti-Wardenaar corer ([Wardenaar, 1987](#)) (core MIS-08-01W), whilst the next few meters were extracted with a Bielorusian corer ([Belokopytov and Veresnevich, 1955](#)) (core MIS-08-01b). The cores were stored at -40°C , and frozen cores were cut at a 1.5 cm sampling interval by a stainless steel band saw at the University of Heidelberg ([Givélet et al., 2004](#)). The sample slices were sub-sampled into two. Half the sample slice was freeze-dried, then mechanically-ground, using an agate ball mill at the University of Liège, to measure the degree of humification, elemental concentrations and Nd and Pb isotope geochemistry. Remaining core samples were stored at -4°C for further analyses, including dating. Peat densities were calculated by weighing a known volume of fresh peat extracted by a cylindrical stainless punch.

Here we focus on the upper 173 cm of peat, i.e., an ombrotrophic section ([Allan et al., 2013c](#)) that covers the past 2500 years (ages reported in [Table 1](#)). The Ca/Mg ratio and Sr concentrations were used to identify the ombrotrophic section as proposed by [Shotyk et al. \(2001\)](#). Note that such geochemical-derived limits are consistent with a biological limit ([Payne, 2011](#)), i.e., a sharp change in the testate amoebae assemblages (Master thesis T. Salpeteur, *unpublished data*).

The building of the age-depth model is described in [Allan et al. \(2013a\)](#). Briefly, it was established by merging cores MIS-08-01W and MIS-08-01b. The chronology was constrained by ^{210}Pb activities measured on the upper 25 cm of peat by alpha spectrometry ([Sikorski and Bluszcz, 2008](#)) at the GADAM Centre (Gliwice, Poland)

Table 1
 Sample depth, density, humification level, age, accumulation rate, historical period, geochemical elementary content (Sc, Ti, REE) and enrichment factor.

Core 01W		Age information					Geochemical data														EF UCC REE/Sc								
Depth cm	Density g/cm ³	HL %	Age yr AD	Error ±yr	AR mm/yr	Period	Sc ppm	Ti ppm	La ppm	Ce ppm	Pr ppm	Nd ppm	Sm ppm	Eu ppm	Gd ppm	Tb ppm	Dy ppm	Ho ppm	Er ppm	Tm ppm	Yb ppm	Lu ppm	La	Nd	Eu	Yb			
a. Data for core MIS-08-1W																													
0.0		14	2008	4	22.1	MP	0.11	113	0.19	0.24	0.03	0.12	0.02	<0.01	0.03	<0.01	0.01	<0.01	0.01	<0.01	<0.01	<0.01	<0.01						
2.2	0.02	7	2007	4	15.0	MP	0.28	33	0.40	0.60	0.07	0.28	0.05	0.01	0.07	0.01	0.04	0.01	0.02	<0.01	0.02	<0.01	0.02	<0.01	0.8	0.6	0.7	0.3	
3.8	0.02	9	2006	4	9.4	MP	0.15	28	0.36	0.53	0.06	0.24	0.05	0.01	0.06	0.01	0.03	0.01	0.02	<0.01	0.02	<0.01	0.02	<0.01	0.7	0.5	0.7	0.4	
4.7	0.03	6	2005	4	8.3	MP	0.17	32	0.39	0.58	0.06	0.25	0.04	0.01	0.07	0.01	0.04	0.01	0.02	<0.01	0.02	<0.01	0.02	<0.01	1.1	0.8	1.0	0.6	
5.6	0.03	12	2004	4	10.4	MP	0.18	33	0.48	0.62	0.07	0.26	0.05	0.01	0.06	0.01	0.04	0.01	0.02	<0.01	0.02	<0.01	0.02	<0.01	1.1	0.8	1.1	0.6	
6.5	0.03	14	2003	4	7.7	MP	0.16	29	0.47	0.58	0.06	0.24	0.04	0.01	0.06	0.01	0.03	0.01	0.02	<0.01	0.01	<0.01	0.02	<0.01	1.2	0.8	1.0	0.7	
7.4	0.03	8	2002	4	11.5	MP	0.17	29	0.43	0.57	0.06	0.24	0.04	0.01	0.06	0.01	0.04	0.01	0.02	<0.01	0.02	<0.01	0.02	<0.01	1.4	0.8	0.9	0.5	
8.3	0.03	12	2001	4	7.0	MP	0.16	31	0.44	0.59	0.07	0.26	0.05	0.01	0.06	0.01	0.04	0.01	0.02	<0.01	0.02	<0.01	0.02	<0.01	1.2	0.8	0.9	0.6	
9.2	0.04	12	2000	4	5.2	MP	0.17	27	0.47	0.62	0.07	0.27	0.04	0.01	0.06	0.01	0.04	0.01	0.02	<0.01	0.02	<0.01	0.02	<0.01	1.3	0.9	0.9	0.7	
10.1	0.04	12	1998	4	7.3	MP	0.16	26	0.45	0.65	0.08	0.29	0.05	0.01	0.07	0.01	0.04	0.01	0.02	<0.01	0.02	<0.01	0.02	<0.01	1.3	0.9	1.0	0.6	
11.0	0.03	12	1997	4	12.3	MP	0.20	26	0.57	0.93	0.11	0.44	0.08	0.02	0.11	0.01	0.06	0.01	0.03	<0.01	0.03	<0.01	0.02	<0.01	1.2	0.9	1.2	0.7	
11.9	0.04	14	1996	4	7.1	MP	0.27	34	0.89	1.54	0.19	0.73	0.13	0.03	0.18	0.02	0.10	0.02	0.06	0.01	0.05	0.01	1.3	1.2	1.5	0.8			
12.8	0.04	15	1995	4	11.5	MP	0.29	54	1.29	2.16	0.26	0.99	0.19	0.04	0.26	0.03	0.15	0.03	0.08	0.01	0.07	0.01	1.5	1.4	1.8	1.1			
13.7	0.07	19	1994	4	2.7	MP	0.37	110	2.13	3.85	0.46	1.77	0.34	0.08	0.45	0.04	0.27	0.05	0.14	0.02	0.12	0.02	2.0	1.8	2.1	1.5			
14.6	0.13	17	1991	4	2.4	MP	0.54	214	3.01	5.68	0.67	2.56	0.47	0.10	0.64	0.06	0.36	0.07	0.20	0.03	0.17	0.02	2.6	2.5	3.1	2.0			
15.5	0.16	18	1987	4	1.4	MP	0.54	260	3.19	6.09	0.71	2.73	0.51	0.11	0.69	0.07	0.40	0.08	0.22	0.03	0.20	0.03	2.5	2.5	2.9	1.9			
16.4	0.16	18	1980	4	1.2	MP	0.47	251	2.96	5.62	0.66	2.49	0.48	0.10	0.63	0.06	0.37	0.07	0.22	0.03	0.18	0.03	2.7	2.6	3.2	2.3			
17.3	0.14	26	1973	4	1.2	MP	0.51	287	3.20	6.14	0.73	2.73	0.50	0.11	0.69	0.07	0.40	0.08	0.23	0.03	0.21	0.03	2.9	2.8	3.3	2.4			
18.2	0.17	29	1965	4	0.7	MP	0.49	294	3.48	6.74	0.79	3.03	0.59	0.12	0.78	0.08	0.44	0.08	0.25	0.03	0.21	0.03	2.9	2.8	3.3	2.5			
19.1	0.19	28	1953	4	0.5	MP	0.44	297	3.71	7.50	0.90	3.43	0.70	0.15	0.90	0.09	0.51	0.10	0.27	0.04	0.24	0.03	3.2	3.2	3.9	2.6			
20.0	0.17	29	1937	4	0.3	RI	0.31	228	3.02	6.21	0.74	2.84	0.60	0.13	0.78	0.08	0.44	0.08	0.24	0.03	0.21	0.03	3.8	4.1	5.2	3.4			
20.9	0.16	32	1901	6	0.2	RI	0.35	225	2.89	5.99	0.72	2.82	0.58	0.13	0.77	0.08	0.46	0.09	0.25	0.03	0.22	0.03	4.4	4.8	6.7	4.2			
21.8	0.17	28	1857	7	0.3	RI	0.40	239	3.06	6.29	0.75	2.88	0.59	0.13	0.79	0.08	0.45	0.09	0.25	0.03	0.21	0.03	3.7	4.2	5.8	3.9			
22.7	0.16	29	1824	25	0.4	RI	0.40	197	2.46	5.06	0.60	2.33	0.47	0.10	0.62	0.06	0.37	0.07	0.19	0.03	0.18	0.03	3.5	3.8	5.2	3.2			
23.6	0.16	23	1802	43	0.7	RI	0.41	211	2.57	5.12	0.59	2.27	0.44	0.10	0.58	0.06	0.33	0.06	0.19	0.03	0.17	0.02	2.8	3.1	3.8	2.8			
24.6	0.15	27	1788	62	1.2	RI	0.43	226	2.26	4.46	0.51	1.94	0.36	0.07	0.50	0.05	0.29	0.05	0.16	0.02	0.15	0.02	2.8	2.9	3.6	2.6			
25.6	0.15	20	1780	82	1.6	RI	0.35	163	1.63	3.12	0.35	1.35	0.26	0.05	0.34	0.04	0.22	0.04	0.13	0.02	0.11	0.02	2.4	2.4	2.7	2.2			
26.6	0.13	21	1774	102	1.1	RI	0.31	135	1.33	2.54	0.39	1.09	0.22	0.04	0.28	0.03	0.17	0.03	0.10	0.01	0.09	0.01	2.1	2.0	2.3	2.0			
28.6	0.14	23	1748	129	0.4	RI	0.31	125	1.22	2.34	0.26	1.01	0.19	0.04	0.25	0.03	0.15	0.03	0.09	0.01	0.08	0.01	2.0	1.8	2.1	1.7			
30.6	0.18	29	1691	120	0.26	Re	0.37	238	2.06	4.16	0.48	1.75	0.33	0.06	0.43	0.04	0.24	0.05	0.14	0.02	0.13	0.02	1.8	1.7	2.1	1.6			
32.6	0.18	33	1611	110	0.22	Re	0.27	155	1.37	2.84	0.32	1.23	0.23	0.05	0.31	0.03	0.18	0.03	0.11	0.01	0.09	0.01	2.5	2.5	2.6	2.1			
34.6	0.16	23	1520	101	0.21	Re	0.27	147	1.23	2.48	0.29	1.09	0.20	0.04	0.27	0.03	0.16	0.03	0.09	0.01	0.08	0.01	2.3	2.4	2.7	2.1			
36.6	0.15	27	1428	91	0.24	Re	0.33	219	1.64	3.33	0.38	1.42	0.27	0.06	0.36	0.04	0.22	0.04	0.13	0.02	0.12	0.02	2.0	2.1	2.2	1.8			
38.6	0.14	30	1348	85	0.30	Re	0.26	160	1.41	2.91	0.33	1.23	0.23	0.05	0.31	0.03	0.18	0.04	0.10	0.01	0.10	0.01	2.3	2.3	2.6	2.2			
40.6	0.12	29	1285	87	0.40	MA	0.29	164	1.52	3.10	0.35	1.32	0.25	0.05	0.34	0.03	0.18	0.04	0.11	0.01	0.10	0.01	2.4	2.4	3.0	2.3			
42.6	0.10	34	1238	89	0.52	MA	0.31	166	1.42	2.76	0.31	1.15	0.22	0.04	0.29	0.03	0.18	0.03	0.11	0.01	0.10	0.02	2.4	2.4	2.6	2.1			
44.6	0.10	28	1202	91	0.68	MA	0.27	134	1.20	2.28	0.25	0.94	0.17	0.03	0.24	0.02	0.14	0.03	0.08	0.01	0.08	0.01	2.1	1.9	2.2	2.0			
46.6	0.10	29	1174	92	0.81	MA	0.29	160	1.16	2.25	0.26	0.94	0.17	0.03	0.23	0.02	0.14	0.03	0.08	0.01	0.08	0.01	2.0	1.8	1.9	1.7			
48.6	0.06	29	1150	94	0.84	MA	0.19	75	0.73	1.33	0.14	0.54	0.10	0.02	0.14	0.01	0.08	0.02	0.04	0.01	0.04	0.01	1.8	1.7	1.7	1.7			
50.6	0.09	30	1125	96	0.75	MA	0.23	115	1.01	1.91	0.21	0.77	0.14	0.03	0.20	0.02	0.12	0.02	0.07	0.01	0.07	0.01	1.7	1.5	1.5	1.4			
52.6	0.09	29	1097	98	0.60	MA	0.20	93	0.79	1.43	0.16	0.58	0.11	0.02	0.15	0.01	0.08	0.02	0.05	0.01	0.05	0.01	2.0	1.8	1.9	1.8			
54.6	0.09	28	1062	100	0.44	MA	0.25	139	1.04	2.00	0.22	0.82	0.15	0.03	0.21	0.02	0.12	0.02	0.08	0.01	0.07	0.01	1.8	1.5	1.6	1.5			
56.7	0.10	23	1015	102	0.42	MA	0.35	235	1.60	3.07	0.34	1.24	0.22	0.04	0.30	0.03	0.18	0.04	0.11	0.02	0.11	0.02	1.9	1.7	1.7	1.8			
58.9	0.10	34	962	105	0.39	MA	0.28	169	1.41	2.71	0.30	1.05	0.20	0.04	0.27	0.03	0.16	0.03	0.10	0.01	0.09	0.01	2.0	1.8	1.9	1.9			
61.1	0.10	31	905	107	0.38	MA	0.23	120	1.03	2.05	0.22	0.80	0.15	0.03	0.20	0.02	0.12	0.02	0.07	0.01	0.06	0.01	2.3	1.9	2.1	1.9			
63.3	0.10	35	848	109	0.39	MA	0.16	68	0.62	1.21	0.13	0.45	0.09	0.02	0.12	0.01	0.07	0.01	0.04	0.01	0.04	0.01	2.0	1.8	1.9	1.7			
65.5	0.09	40	793	111	0.42	MA	0.18	82	0.75	1.45	0.16	0.55	0.10	0.02	0.14	0.01	0.08	0.02	0.05	0.01	0.04	0.01	1.8	1.5	1.7	1.5			
67.7	0.09	39	742	114	0.48	MA	0.22	96	0.76	1.50	0.16	0.59	0.10	0.02	0.15	0.02	0.09	0.02	0.06	0.01	0.05	0.01	1.9	1.6	1.8	1.5			
69.9	0.09	35	698	116	0.59	MA	0.18	96	0.73	1.45	0.16	0.58	0.10	0.02	0.15	0.01	0.09	0.02	0.05	0.01	0.05	0.01	1.6	1.4	1.6	1.5			

(continued on next page)

Table 1 (continued)

72.1	0.08	37	663	117	0.74	MA	0.17	68	0.61	1.21	0.14	0.50	0.09	0.02	0.13	0.01	0.07	0.01	0.04	0.01	0.04	0.01	0.04	<0.01	1.8	1.6	1.9	1.7	
74.3	0.08	37	635	118	0.94	MA	0.10	40	0.36	0.73	0.08	0.29	0.06	0.01	0.08	0.01	0.04	0.01	0.03	<0.01	0.02	<0.01	1.6	1.5	1.7	1.4	1.5	1.7	1.4
76.5	0.09	42	613	119	1.20	MA	0.12	49	0.40	0.80	0.09	0.34	0.06	0.01	0.09	0.01	0.05	0.01	0.03	<0.01	0.02	<0.01	1.7	1.5	2.1	1.4	1.5	2.1	1.4
78.7	0.08	45	595	120	1.50	MA	0.12	43	0.38	0.73	0.09	0.31	0.06	0.01	0.08	0.01	0.05	0.01	0.03	<0.01	0.02	<0.01	1.5	1.5	1.9	1.3	1.5	1.9	1.3
80.9	0.10	48	581	121	1.79	MA	0.12	49	0.48	0.95	0.11	0.40	0.08	0.02	0.10	0.01	0.06	0.01	0.03	<0.01	0.03	<0.01	1.4	1.3	1.8	1.2	1.3	1.8	1.2
83.1	0.10	46	569	122	1.96	MA	0.17	79	0.66	1.28	0.14	0.52	0.10	0.02	0.14	0.01	0.07	0.02	0.05	<0.01	0.04	<0.01	1.8	1.7	2.0	1.5	1.7	2.0	1.5
85.3	0.10	43	558	124	1.92	MA	0.15	60	0.61	1.18	0.13	0.46	0.09	0.02	0.12	0.01	0.06	0.01	0.04	<0.01	0.03	<0.01	1.8	1.6	1.9	1.4	1.6	1.9	1.4
87.5	0.08	43	546	125	1.69	MA	0.13	44	0.40	0.80	0.09	0.29	0.06	0.01	0.07	0.01	0.04	0.01	0.02	<0.01	0.02	<0.01	1.8	1.6	1.6	1.3	1.6	1.6	1.3
89.7	0.07	38	533	126	3.13	MA	0.16	66	0.49	0.96	0.11	0.38	0.07	0.01	0.10	0.01	0.06	0.01	0.03	<0.01	0.03	<0.01	1.4	1.2	1.5	1.0	1.2	1.5	1.0
b. Data for core MIS-08-01B																													
Core 01B																													
Age information																													
Geochemical data																													
EF UCC REE/Sc																													
94.5	0.06	51	498	129	0.93	MA	0.13	42	0.34	0.66	0.08	0.28	0.05	0.01	0.07	0.01	0.04	0.01	0.02	<0.01	0.02	<0.01	1.4	1.3	1.3	1.2	1.1	1.3	1.0
97.6	0.06	51	465	131	0.85	MA	0.11	29	0.29	0.57	0.06	0.22	0.04	0.01	0.06	0.01	0.03	0.01	0.02	<0.01	0.01	<0.01	1.2	1.1	1.3	1.0	1.0	1.2	0.8
102.1	0.06	30	408	134	0.73	MA	0.14	32	0.31	0.59	0.06	0.23	0.04	0.01	0.06	0.01	0.03	0.01	0.02	<0.01	0.02	<0.01	1.2	1.0	1.2	0.8	1.0	1.0	0.8
105.2	0.07	46	365	137	0.68	MA	0.13	57	0.44	0.84	0.09	0.33	0.06	0.01	0.09	0.01	0.05	0.01	0.03	<0.01	0.03	<0.01	1.0	0.9	1.0	0.8	0.9	1.0	0.8
108.2	0.06	36	319	139	0.65	MA	0.19	71	0.58	1.10	0.13	0.46	0.08	0.02	0.12	0.01	0.07	0.01	0.04	0.01	0.04	0.01	1.5	1.3	1.7	1.5	1.3	1.7	1.5
109.7	0.07	33	296	140	0.64	RP	0.18	66	0.58	1.12	0.13	0.47	0.09	0.02	0.12	0.01	0.07	0.01	0.04	0.01	0.04	0.01	1.4	1.3	1.3	1.3	1.3	1.3	1.3
111.2	0.07	31	272	141	0.63	RP	0.20	88	0.62	1.18	0.13	0.48	0.09	0.02	0.12	0.01	0.08	0.02	0.05	0.01	0.04	0.01	1.5	1.4	1.6	1.4	1.4	1.6	1.4
112.7	0.07	40	248	142	0.58	RP	0.14	70	0.54	1.04	0.12	0.43	0.08	0.01	0.10	0.01	0.07	0.01	0.04	0.01	0.04	0.01	1.4	1.2	1.4	1.3	1.2	1.4	1.3
114.3	0.07	38	222	139	0.62	RP	0.22	108	0.76	1.50	0.17	0.66	0.12	0.02	0.17	0.02	0.10	0.02	0.06	0.01	0.05	0.01	1.8	1.6	1.6	1.7	1.6	1.6	1.7
117.3	0.07	29	173	132	0.62	RP	0.16	59	0.50	0.96	0.11	0.41	0.07	0.02	0.10	0.01	0.06	0.01	0.04	<0.01	0.03	<0.01	1.5	1.6	1.6	1.5	1.6	1.6	1.5
120.3	0.07	38	124	126	0.63	RP	0.14	84	0.74	1.45	0.16	0.60	0.10	0.02	0.14	0.02	0.09	0.02	0.05	0.01	0.05	0.01	1.4	1.3	1.5	1.2	1.3	1.5	1.2
124.9	0.07	35	51	116	0.66	RP	0.23	138	1.10	2.24	0.25	0.94	0.19	0.04	0.24	0.02	0.15	0.03	0.08	0.01	0.08	0.01	2.3	2.2	2.4	2.0	2.2	2.4	2.0
127.9	0.07	42	6	110	0.69	RP	0.19	154	1.20	2.39	0.27	1.02	0.18	0.04	0.25	0.03	0.16	0.03	0.09	0.01	0.08	0.01	2.2	2.2	2.5	2.0	2.2	2.5	2.0
129.4	0.07	47	-16	106	0.72	RP	0.20	109	0.88	1.77	0.20	0.74	0.15	0.03	0.19	0.02	0.12	0.02	0.07	0.01	0.06	0.01	2.9	2.8	3.3	2.7	2.8	3.3	2.7
130.9	0.07	45	-37	103	0.74	RP	0.16	70	0.60	1.23	0.14	0.54	0.11	0.02	0.14	0.01	0.08	0.02	0.04	0.01	0.04	0.01	2.0	2.0	2.2	2.0	2.0	2.2	2.0
132.4	0.07	40	-58	100	0.73	RP	0.16	58	0.61	1.27	0.15	0.56	0.10	0.02	0.14	0.01	0.08	0.02	0.04	0.01	0.04	0.01	1.7	1.7	2.1	1.5	1.7	2.1	1.5
134.0	0.07	42	-78	96	0.81	RP	0.17	52	0.54	1.12	0.13	0.50	0.10	0.02	0.12	0.01	0.08	0.01	0.04	0.01	0.03	<0.01	1.7	1.8	2.2	1.5	1.8	2.2	1.5
135.0	0.06	nd	-91	94	0.84	RP	0.16	60	0.65	1.33	0.15	0.56	0.11	0.02	0.14	0.01	0.08	0.02	0.04	0.01	0.04	0.01	1.4	1.5	2.1	1.3	1.5	2.1	1.3
135.5	0.07	nd	-97	93	0.86	RP	0.13	60	0.59	1.19	0.14	0.51	0.09	0.02	0.13	0.01	0.08	0.01	0.04	0.01	0.04	0.01	1.8	1.8	2.1	1.5	1.8	2.1	1.5
138.0	0.06	nd	-126	97	0.94	RP	0.18	65	0.59	1.15	0.13	0.48	0.10	0.02	0.12	0.01	0.08	0.01	0.04	0.01	0.04	0.01	2.1	2.1	2.6	1.8	2.1	2.6	1.8
138.5	0.09	nd	-131	98	0.87	RP	0.14	73	0.50	0.96	0.11	0.39	0.07	0.01	0.10	0.01	0.07	0.01	0.04	0.01	0.04	0.01	1.5	1.4	1.6	1.4	1.4	1.6	1.4
139.5	0.06	38	-142	100	2.44	RP	0.16	69	0.47	0.90	0.10	0.37	0.07	0.01	0.09	0.01	0.06	0.01	0.03	<0.01	0.03	<0.01	1.6	1.4	1.5	1.6	1.4	1.5	1.6
142.6	0.06	nd	-158	102	1.04	RP	0.12	27	0.26	0.52	0.06	0.21	0.04	0.01	0.05	0.01	0.03	0.01	0.02	<0.01	0.02	<0.01	1.3	1.2	1.4	1.3	1.2	1.4	1.3
145.6	0.05	38	-187	103	1.14	RP	0.12	23	0.24	0.47	0.05	0.19	0.03	0.01	0.05	0.01	0.03	0.01	0.02	<0.01	0.02	<0.01	1.0	0.9	0.9	0.9	0.9	0.9	0.9
148.6	0.05	26	-213	100	1.24	RP	0.13	34	0.34	0.66	0.07	0.26	0.05	0.01	0.07	0.01	0.04	0.01	0.02	<0.01	0.02	<0.01	0.9	0.8	1.0	0.8	0.8	1.0	0.8
151.7	0.06	35	-238	97	1.32	RP	0.16	40	0.38	0.74	0.08	0.31	0.06	0.01	0.08	0.01	0.04	0.01	0.03	<0.01	0.02	<0.01	1.2	1.1	1.3	1.0	1.1	1.3	1.0
154.7	0.07	37	-260	94	0.69	RP	0.20	115	0.79	1.56	0.17	0.65	0.11	0.03	0.16	0.02	0.10	0.02	0.06	0.01	0.06	0.01	1.0	1.0	1.1	0.9	1.0	1.1	0.9
157.7	0.06	30	-293	89	1.32	RP	0.16	47	0.39	0.77	0.09	0.31	0.06	0.01	0.08	0.01	0.05	0.01	0.03	<0.01	0.02	<0.01	1.8	1.7	1.9	1.7	1.7	1.9	1.7
160.8	0.05	25	-315	86	1.38	RP	0.12	24	0.23	0.47	0.05	0.19	0.03	0.01	0.05	0.01	0.03	<0.01	0.01	<0.01	0.02	<0.01	1.1	1.0	1.2	0.9	1.0	1.2	0.9
163.8	0.06	21	-337	83	1.33	RP	0.14	27	0.29	0.56	0.06	0.24	0.05	0.01	0.06	0.01	0.04	0.01	0.02	<0.01	0.02	<0.01	0.9	0.8	1.0	0.8	0.8	1.0	0.8
165.3	0.05	nd	-349	81	1.30	RP	0.22	21	0.22	0.45	0.05	0.20	0.03	0.01	0.05	0.01	0.03	0.01	0.02	<0.01	0.02	<0.01	0.9	0.9	1.1	0.9	0.9	1.1	0.9
166.8	0.05	28	-360	83	1.27	RP	0.13	25	0.27	0.51	0.06	0.21	0.04	0.01	0.05	0.01	0.03	0.01	0.02	<0.01	0.02	<0.01	0.5	0.5	0.6	0.4	0.5	0.6	0.4
169.9	0.05	28	-385	86	1.21	RP	0.10	25	0.27	0.52	0.06	0.22	0.04	0.01	0.06	<0.01	0.03	0.01	0.02	<0.01	0.01	<0.01	0.9	0.9	1.1	0.7	0.9	1.1	0.7
172.9	0.05	33	-411	89	1.16	pre-RP	0.14	30	0.31	0.63	0.07	0.27	0.05	0.01	0.07	0.01	0.04	0.01	0.02	<0.01	0.02	<0.01	1.3	1.2	1.5	0.9	1.2	1.5	0.9
175.9	0.06	44	-437	92	1.12	pre-RP	0.14	51	0.40	0.80	0.09	0.33	0.06	0.01	0.09	0.01	0.06	0.01	0.03	<0.01	0.03	<0.01	1.0	1.0	1.2	0.8	1.0	1.2	0.8
179.0	0.07	37	-465	95	1.09	pre-RP	0.13	57	0.36	0.69	0.08	0.28	0.05	0.01	0.07	0.01	0.05	0.01	0.03	<0.01	0.02	<0.01	1.3	1.3	1.5	1.3	1.3	1.5	1.3
180.5	0.07	29	-479	97	1.08	pre-RP	0.26	125	0.77	1.55	0.17	0.65	0.11	0.03	0.18	0.02	0.11	0.02	0.06	0.01	0.06	0.01	1.2	1.1	1.3	1.1	1.1	1.3	1.1
183.5	0.07	37	-507	100	3.62	pre-RP	0.15	53	0.45	0.86	0.10	0.36	0.07	0.01	0.09	0.01	0.05	0.0											

and ten ^{14}C dates of extracted peat macroremains by Acceleration Mass Spectrometer (AMS). The ^{14}C samples have been prepared according to protocol by Piotrowska (2013) at the GADAM Centre. For the upper part, ^{210}Pb age dates were derived using the CRS model (Appleby, 1978). To build the final age-depth model, ^{210}Pb and ^{14}C data were processed using *Bacon* software (Blaauw and Christen, 2011).

The humification degree (HD) was measured by a colorimetric method using an Aldrich spectrophotometer (Station Scientifique des Hautes Fagnes) on alkaline peat extracts, according to protocols given in Chambers et al. (2011). About 200 mg of dried and powdered peat samples were mixed with 100 ml of NaOH (8%), and the solution was boiled for 1 h. After cooling, the solution was brought to 200 ml with MQ distilled water, homogenized and filtered using Whatman ($n^{\circ}1$) filter paper. Before measurement, 50 ml of solution was taken and diluted with 50 ml of MQ distilled water. A standard with a humification level of 100% (Humic acid technical, ALDRICH) was included in the measurement. The absorbance was measured at 540 nm. The humification percentage was derived from the ratio between the absorption values in peat samples and standard.

Elemental geochemical measurements were made on 200 mg of dried and powdered peat samples after digestion at high pressure (120 bars) and high temperature (240 °C) in a microwave autoclave in Germany (Institute of Geochemistry Environmental, University of Heidelberg) following Krachler et al. (2002). Peat samples, blanks and vegetation standards were dissolved in 3 ml HNO_3 (65%, analytical-reagent grade and further purified by sub-boiling distillation) and 0.1 ml HBF_4 (50%, purum). The digestion of organic matter was improved by introducing H_2O_2 vapours from the base cup of the device. After digestion, 3 ml of solution was transferred to a Falcon tube then filled up to 14 ml. In Toulouse, an aliquot of 500 μl was transferred into a new Falcon tube and diluted with 10 ml of HNO_3 (2%, ultrapure) and 100 μg of an In-Re internal standard solution. Ti, Sc and Rare Earth Element (REE) contents were measured by a Quadrupole Inductively Coupled Plasma Mass Spectrometry (Q-ICP-MS 7500 Agilent (Observatoire Midi-Pyrénées, Toulouse). The Agilent 7500 ce is equipped by a collision cell allowing to minimize interferences. Blank concentrations of diluted solutions are negligible, representing usually less than 0.1% of the digested diluted peat solutions. The limits of quantification were calculated from the intensity and standard deviation measurements of 6 blanks. They range between a few pg g^{-1} for La, one hundred pg g^{-1} for Nd, and a few ng g^{-1} for Pb and Ti. Such limits of detection are in the range or lower than published ICP-MS values: \leq a few tens of ng g^{-1} for the light REE La-Gd and $<$ a few ng g^{-1} for the heavy REE Tb-Lu (Ferrat et al., 2012a,b). These are two orders of magnitude below the minimum concentrations measured for La, and in general one order of magnitude for Nd and Pb. The accuracy of the measurements, deduced from measurements of three certified plant standards (*ICHTJ* CTA-OTL-1 Oriental Tobacco Leaves, *NIST* Tomato Leaves 1573 and *IAEA* Lichen 336), ranges within 80–98% for REE (i.e., 82–98%

for La, 80–98% for Ce; 94% for Nd, 81–96% for Sm, 92–95% for Eu, 97% for Gd, 89% for Lu), and 92–97% for Pb. The reproducibility of the measurements is estimated by repeated measurements of 3 peat samples. The reproducibility averages 96% for La & Pb, and 98% for Ti. Corrections for isobaric interferences due to the formation of polyatomes (mainly Ce, La, Nd and Pr oxides) have been taken into account to obtain accurate trace element quantification and in particular for Eu and Gd (e.g., Meisel et al., 2002). For the Agilent 7500 ce*, we correct for example the measurement for the three Gd isotopes (^{156}Gd , ^{157}Gd and ^{158}Gd) using well-known corrections for interferences (i.e., ^{156}Gd for $^{140}\text{Ce-}^{16}\text{O}$ and $^{139}\text{La-}^{16}\text{O-H}^+$; ^{157}Gd for $^{141}\text{Pr-}^{16}\text{O}$ and $^{140}\text{Ce-}^{16}\text{O-H}^+$; ^{158}Gd for $^{142}\text{Nd-}^{16}\text{O}$ & $^{141}\text{Pr-}^{16}\text{O-H}^+$).

Radiogenic isotope pretreatments were carried out in a class-100 clean laboratory at ULg. Between 0.1 and 1 g of dried peat were placed 6 h into an oven at 550 °C to remove by combustion all organic matter (Chambers et al., 2011). After calcination, the samples were dissolved on a hot-plate (125 °C) in 4 ml of HF (40%, 23 N) and 1 ml of HNO_3 (65%, 14 N). The solution was evaporated to dryness and the residue was re-dissolved in 2 ml of HCl (6 N). All acids were of analytical reagent grade, further purified by sub-boiling distillation in PTFE vials. After evaporation, the sample was dissolved in 500 μl HBr 0.8 N and loaded on an HCl-preconditioned column with AG1-X8 (200–400 mesh) exchanging resin. Most cations, and REE in particular, were first eluted by 4 ml of HBr 0.8 N. Then Pb was eluted by 2 additional ml of HCl 6 N. The Pb-enriched solution was evaporated and kept in a Teflon vial until measurement. Nd was purified by a two-step column separation procedure. The REE-enriched solution was evaporated, dissolved in 500 μl HNO_3 2 N and then loaded onto a HNO_3 -preconditioned column with TRU-spec 50–100 μm resin. After repeated column cleaning with HNO_3 2 N (7×0.5 ml), the REE were collected by passing 2.5 ml of diluted HNO_3 (0.05 N). This solution was directly loaded onto a preconditioned and precalibrated Ln-spec column following the modified scheme proposed by Mikova and Denkova (2007). The REE were sequentially eluted by HCl 0.25 N, Nd was collected after passing 2.75–3 ml. The Nd-enriched solution was evaporated and kept in a Teflon vial until measurement. The Nd and Pb isotope compositions were determined in static wet (Pb) or dynamic dry (Nd) mode on a Multi Collector-Inductively Coupled Plasma Mass Spectrometer (MC-ICP-MS) Nu plasma at ULB in Brussels. The instrumental drift was controlled by standard bracketing using NBS981 standard data (Galer and Abouchami, 1998) for Pb and the Rennes standard data (Chauvel and Blichert-Toft, 2001) for Nd. Repeated standard measurements (for NBS981: $^{208}\text{Pb}/^{204}\text{Pb}$ 36.7130 ± 0.0032 , $^{207}\text{Pb}/^{204}\text{Pb}$ 15.4958 ± 0.0012 , $^{206}\text{Pb}/^{204}\text{Pb}$ 16.9390 ± 0.0012 , $n = 41$; for Rennes standard: $^{143}\text{Nd}/^{144}\text{Nd} = 0.511957 \pm 0.000033$, $n = 99$) are consistent with the recommended values and are in agreement with the laboratory long term values ($^{208}\text{Pb}/^{204}\text{Pb}$ 36.709 ± 0.021 , $^{207}\text{Pb}/^{204}\text{Pb}$ 15.4951 ± 0.0066 , $^{206}\text{Pb}/^{204}\text{Pb}$ 16.9392 ± 0.0006 , $n = 350$; $^{143}\text{Nd}/^{144}\text{Nd} = 0.511946$, $n = 750$). Mass fractionation for Pb was corrected by using Tl as an

internal standard. Measured $^{143}\text{Nd}/^{144}\text{Nd}$ ratios were corrected for mass fractionation using the $^{146}\text{Nd}/^{144}\text{Nd}$ values. The standardized and mass fractionation corrected $^{143}\text{Nd}/^{144}\text{Nd}$ ratios were expressed as ϵNd , as follows: $\epsilon\text{Nd} = [({}^{143}\text{Nd}/^{144}\text{Nd} \text{ corr.} - 0.512638)/0.512638] \times 10000$ with 0.512638 as the chondritic uniform reservoir (CHUR, data from [Wasserburg et al., 1981](#)) representing the bulk earth composition. For Nd, 2 duplicates give consistent results within 0.1–0.3 ϵNd ; 4 replicates, analysed in wet mode, are consistent within 0.1–0.4 ϵNd ([Table 2a](#)).

3. RESULTS

3.1. REE content

All REE display similar depth profiles. We report La and Nd as Light Rare Earth Elements (LREE), Eu as Middle Rare Earth Elements (MREE) and Yb as Heavy Rare Earth Elements (HREE) ([Fig. 1](#), [Table 1](#)). The REE vary in parallel with the lithogenic elements such as Sc or Ti (e.g., coefficient correlation $R^2 = 0.83$ for Nd–Ti, 0.84 for La–Ti, 0.86 for Ce–Ti and 0.87 for Yb–Ti). Such trends demonstrate the conservative behavior of the REE in the peat sedimentary record, as previously demonstrated by [Yliruokanen and Lehto \(1995\)](#) and later by [Krachler et al. \(2003\)](#). For instance, the La content ranges between 0.19 and $3.7 \mu\text{g g}^{-1}$. Similar range of composition was observed in the Black Forest peat record ($0.26 < \text{La} < 3.4$). The La content increases in the upper 50 cm, and the highest content is reached at 19 cm (1965 AD, [Table 1a](#)). The La content then decreases in the upper 10 cm (age younger than 1998 AD). At the

surface, where there are living *Sphagnum* mosses, the value (0.19) is close to the preanthropogenic value ($0.28 \mu\text{g g}^{-1}$) measured at the base of the peat profile (753 cm, ca. 5500 BC, [Allan et al., 2013c](#)).

REE content has been normalized to the Upper Continental Crust (UCC – [McLennan, 2001](#)). All crustal-normalized REE patterns are flat, with a slight enrichment in Gd. For instance we report REE patterns ([Fig. 2](#)) for 3 peat samples characterized by different REE content: a REE-poor sample at the base of the studied peat section (169 cm, 400 BC, pre-Roman Period); an intermediate REE-rich sample (129 cm, 50 AD, Roman Period, [Table 1b](#)) and a REE-rich sample (21 cm, 1900 AD, Industrial Revolution). Note the REE pattern at the base of the peat record (i.e., mean of the samples analysed between 700 and 750 cm, minerotrophic peat, age < 5500 BC – [Allan et al., 2013c](#)) display a similar profile but with a lower LREE content.

3.2. Nd and Pb isotopic signatures

The Misten ϵNd signatures vary between -13 and -10 , the $^{206}\text{Pb}/^{207}\text{Pb}$ isotope ratios range between 1.15 and 1.19 ([Table 2a and b](#), [Fig. 3a](#)). In spite of the narrow range of ϵNd variation, some temporal trends are evident. The samples cluster in 4 groups according to their age interval: Iron Age and Roman Period (400 BC–300 AD, 173–108 cm); Middle Age (500–1300 AD, 87–40 cm); Industrial Revolution 1700–1950 AD, 29–20 cm); Contemporary period, here referred as “Modern Period”, (1973–2007 AD, upper 19 cm). In [Fig. 3a](#) the Middle Age samples are characterized by the highest $^{206}\text{Pb}/^{207}\text{Pb}$ ratios (up to 1.19) and the most

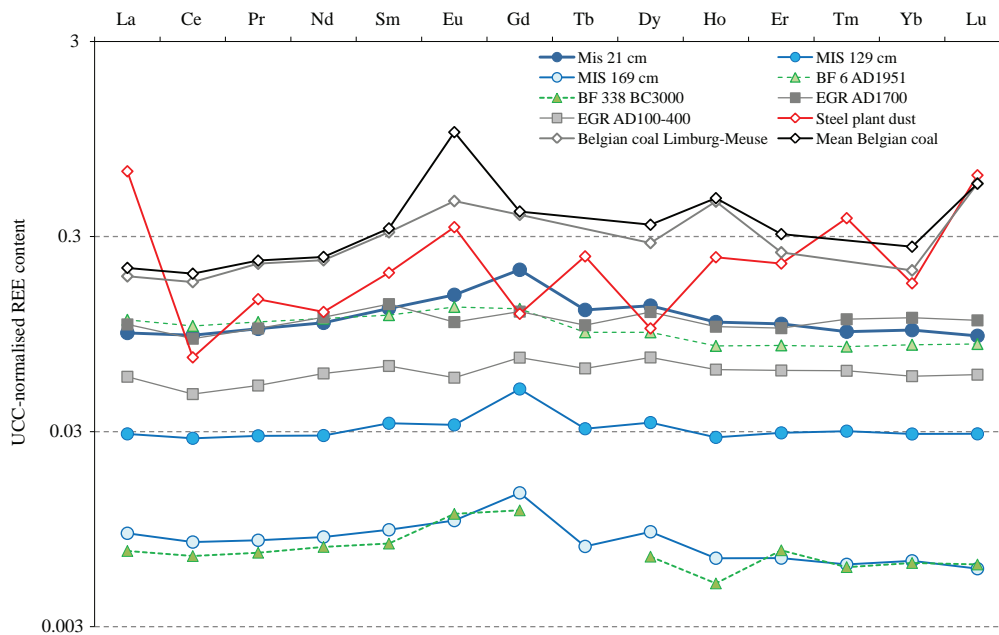


[Fig. 2](#). UCC-normalised REE pattern. Circle: Misten data; square: Black Forest data ([Aubert et al., 2006](#)); diamond: Etang de la Gruyère data, Switzerland ([Krachler et al., 2003](#)). The REE patterns for Belgian coals (grey diamond) from three main ores (data from Camille Delvigne, pers. comm. 2011) and the signature for steel plant dust (large diamond – data from [Geagea et al., 2007](#)) is plotted for comparison. Misten data from [Table 1](#).

negative Nd signatures (down to -13). The more negative Nd excursion, confirmed by a replicate measurement, is observed for the 1000 AD sample. The Roman $^{206}\text{Pb}/^{207}\text{Pb}$ ratios range between 1.173 and 1.181, the ϵNd between -11 and -12 . The $^{206}\text{Pb}/^{207}\text{Pb}$ signatures shift during the Industrial Revolution from 1.176 to 1.155. The Pb isotopic data for the Modern period remain within the same range of variation. The Nd peat signatures become less negative during the Industrial Revolution with values close to -11 since 1800 AD as well as during the Modern Period (with less negative signatures at 1998 and 2007 AD, with $\epsilon\text{Nd} = -10$). The shift in the Pb isotopic data is linked with a significant enrichment in Pb content since the Industrial Revolution (Fig. 3b).

4. DISCUSSION

4.1. Misten REE deposition and comparison with other European peat records

Based on the sediment accumulation rate, the peat density and the sum of REE, we calculate the total accumulation rate (AR) of REE for each sample, as follows:

$$\text{AR}_X \text{ in } \text{mg m}^{-2} \text{y}^{-1} = [\text{X}] \text{ in } \mu\text{g g}^{-1} \times \text{peat density in } \text{g cm}^{-3} \times \text{peat growth rate in } \text{cm y}^{-1} \times 10$$

The AR ranges between 0.02 and $4.7 \text{ mg m}^{-2} \text{ yr}^{-1}$, remaining lower than $0.5 \text{ mg m}^{-2} \text{ yr}^{-1}$ for most of the peat record (Fig. 4). As an exception, we note a slight and brief increase during the Middle Ages (~ 560 AD, 83–85 cm, Table 1a) and a pronounced increase since the Industrial Revolution (<30 cm). The highest accumulation rate is reached at 15 cm (~ 1990 AD), then it decreases toward the peat surface and remains stable within the upper 10 cm (age younger than 1998 AD).

Comparisons between our record with previously published peat data recorded from Europe and shown in Fig. 2. All REE patterns from peat samples are marked by relatively flat UCC-normalized patterns without any significant fractionation between LREE and HREE. It is notable that data from the Black Forest in Germany (BF – Aubert et al., 2006) display the largest range of variation. The range of variation is narrow in the Swiss samples from Etang de la Gruère (ETG, Krachler et al., 2003) but its REE-richest sample is consistent with the two other European records.

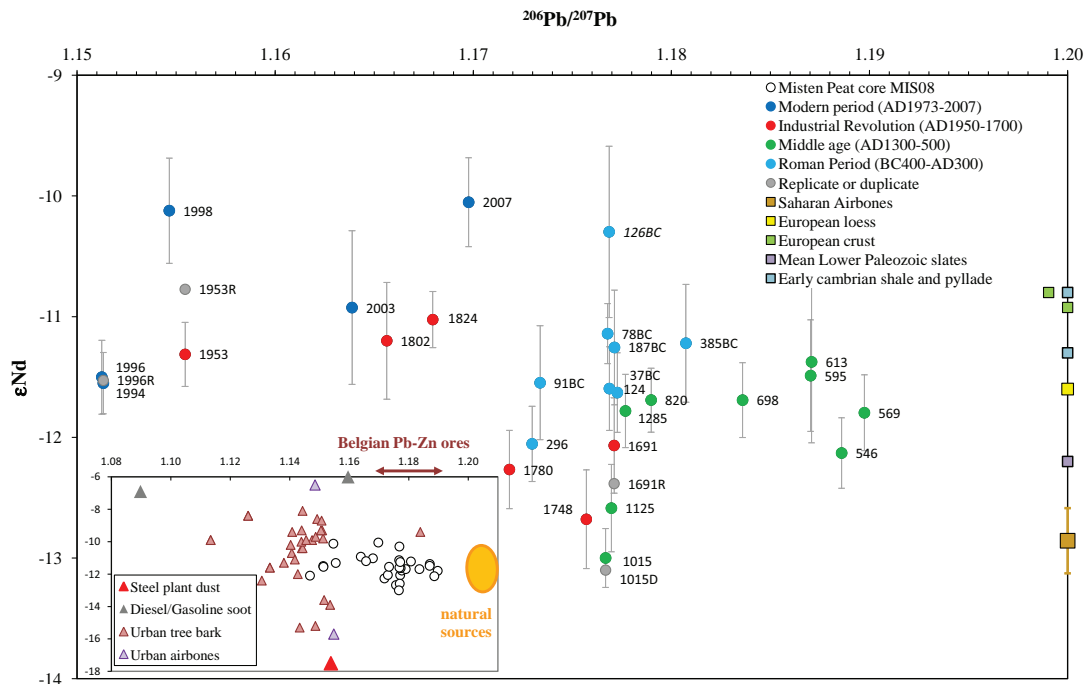


Fig. 3a. ϵNd vs. $^{206}\text{Pb}/^{207}\text{Pb}$. Dots: Misten peat samples (data in Tables 2a and b). Colors according to age interval: blue, Roman and Late Roman Period (400BC–300AD, 173–108 cm); green, Middle Ages (500–1300AD, 87–40 cm); red, Industrial Revolution 1700–1950AD, 29–20 cm); dark blue, Modern Period (1973–2007AD, upper 19 cm). Grey dots: replicate and duplicate analyses (see Table 1). The vertical bars indicate the 2 sigma error bars on the Nd isotope measurement. Isotope Pb data for the Industrial Revolution and Modern period are from Allan et al. (2013a). Natural and anthropogenic dust sources are also reported. Squares: Isotope signature of potential local (Early Cambrian shales = -11.3 , André et al., 1986; mean Paleozoic shales = -12.2 , Linnemann et al., 2012), regional (European loess from Belgium, France and England – Gallet et al., 1998; European soils, geochemical atlas – <http://www.gtk.fi/publ/foregsatlas/>) or global natural dust sources (Saharan airbornes, Grousset et al., 1988a,b; Goldstein et al., 1984; Colin, 1993; Henry et al., 1994). Note the $^{206}\text{Pb}/^{207}\text{Pb}$ ratio for the natural dust sources is fixed at 1.20, if no Pb isotope available data. The lower panel reports the Misten peat data (dots) with regard to the signature of the main anthropogenic sources (triangles): Steel plant dust (Geagea et al., 2007); diesel and gasoline soot (Geagea et al., 2008a); urban airbornes (Geagea et al., 2008a); urban tree bark (Geagea et al., 2007, 2008a, 2008b) and regional Belgian and German Pb–Zn ores (Dejonghe, 1998; Durali-Mueller et al., 2007). All data, except for urban tree bark, are reported in Table 3. (For interpretation of the references to color in this figure legend, the reader is referred to the web version of this article.)

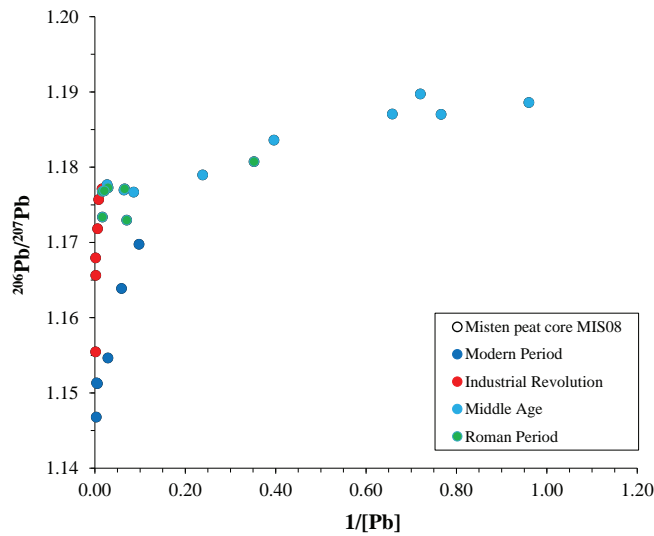


Fig. 3b. Binary diagram 1/Pb content and $^{206}\text{Pb}/^{207}\text{Pb}$. Same color code than for Fig. 3a. Data from Table 2b. A Pb-enrichment is observed in the Industrial Revolution and Modern samples. This enrichment is associated with a significant shift in the Pb isotopic ratios, underlining the major human influence in the trace metal dust supplies to the Misten bog over the last 300 years.

Since all REE display similar trends, we compared the La accumulation rates of the Misten with the two European peat records. The pre-industrial values calculated for Black Forest ($\sim 0.02 \text{ mg m}^{-2} \text{ yr}^{-1}$, Aubert et al., 2006) or for EGR ($\sim 0.08 \text{ mg m}^{-2} \text{ yr}^{-1}$, Krachler et al., 2003) at 1800 AD are consistent with the lowest value measured at the base of the Misten record ($0.02 \text{ mg m}^{-2} \text{ yr}^{-1}$ at

5500 BC, age from Allan et al., 2013c). In the three records, a significant increase is observed during the Industrial Revolution. At 1950 AD the three records are supplied by a similar range of accumulation rates of La, estimated from 0.20 to $0.30 \text{ mg m}^{-2} \text{ yr}^{-1}$. Then the La accumulation rate remains stable (EGR) or it slightly decreases (BF). The next (1990s) increase is not recorded in BF or EGR but the

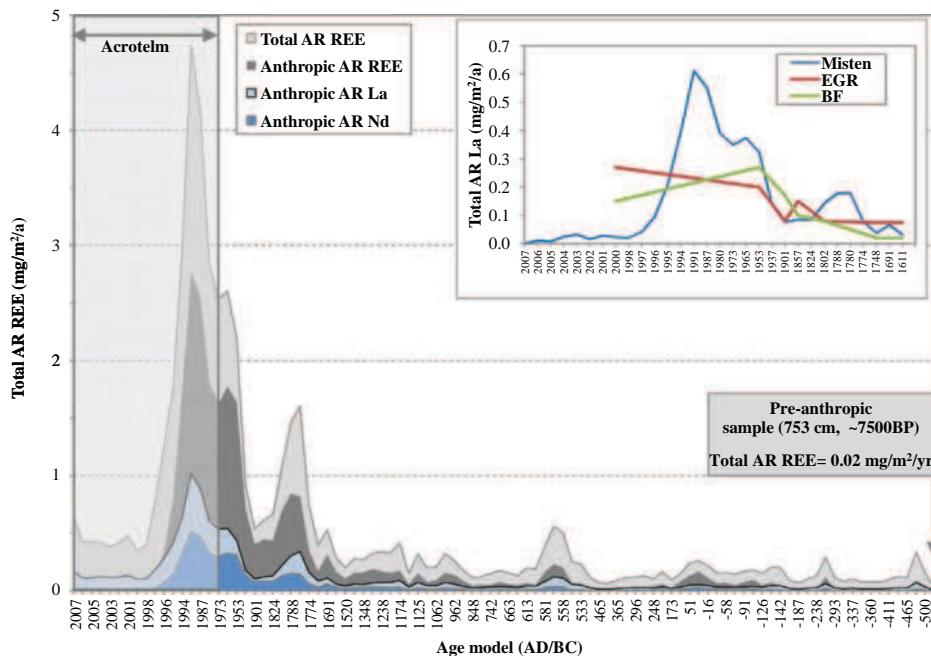


Fig. 4. Estimated accumulation rate (AR) of REE and evolution through the last 2500 years. Total (i.e., natural + anthropogenic) and anthropogenic AR for La, Nd and sum REE are reported versus age model. Accumulation rates are calculated from peat density, accumulation rate and elementary content (data in Table 1). The grey interval corresponds to the acrotelm peat section. The pre-anthropogenic REE AR measured at the base of the Misten peat accumulation (753 cm, 7500 BP) is reported for reference. La AR for Germany (BF, Aubert et al., 2006) and Switzerland (EGR, Krachler et al., 2003) are reported in comparison with Misten data EGR in the upper panel.

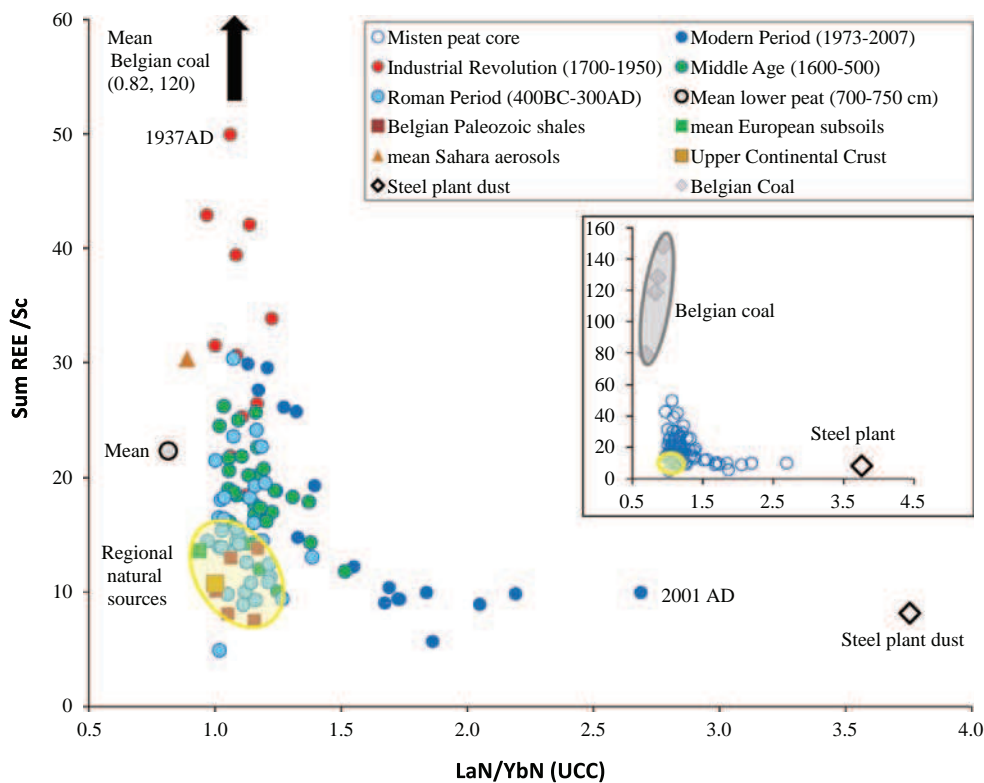


Fig. 5. Sum REE/Sc vs. La_N/Yb_N . The sum of REE normalized to Sc as a lithogenic natural reference is plotted in regard with the UCC-normalized La/Yb (La_N/Yb_N) ratios. Data calculated from Table 1. The mean value for the lower minerotrophic section of the Misten record (753 cm, 7500 BP) is also reported. Belgian Paleozoic shales (André et al., 1986, European subsoil (data from geochemical atlas – <http://www.gtk.fi/publ/foregsatlas/>) and UCC (McLennan, 2001) are reported to define the field of regional natural sources. Note the signature of the base of the peat (mean 700–750 cm, older than 5500 BC years, age from Allan et al., 2013c) is enriched in REE compared to UCC and with the mean signature for Belgian Paleozoic shales (mean 10.8), reflecting the peculiar local geological basement (mainly Early Cambrian quartzite – Verniers et al., 2001). Mean value for Saharan airbornes represents the distal natural supplies (data from Moreno et al., 2006). The average signature for Belgian coal (grey diamond, data from Camille Delvigne, pers. comm. 2011) and steel plant dust from area (data from Geagea et al., 2007) are also reported for comparison. The insert panel reports the Misten data (dots) in regard with the field of Belgian coal, steel plant dust and natural sources.

sample resolution is different, with no data available between 1953 and 2000 AD (Fig. 4, upper panel).

4.2. Natural versus anthropogenic contribution in REE deposition

In the Misten record the REE deposition displays significant changes over time (Fig. 4). Such changes could be the result of natural (e.g., large increase in long-range dust fluxes) and/or anthropogenic dust contribution. To estimate any excess in the REE deposition in the Misten peat record, we calculate a REE enrichment factor (EF) relative to the signature of the Upper Continental Crust (McLennan, 2001) as follows: $EF = (REE/Sc)_{sample} / (REE/Sc)_{UCC}$. All REE display similar EF profiles (Table 1, see also Supplementary data SM2). Individual REE EF >2 are observed between 125 and 130 cm (10 BC–50 AD, Roman Period, Table 1b), from 45 cm (1174 AD, Middle Ages, Table 1a) to 10 cm (1998 AD). The highest EF (9) is reached at 19 cm (1954 AD, Table 1a). The upper section EF then decreases to values lower than the preanthropogenic signature (EF 1.3 at 753 cm, see upper panel in SM2). Note the pre-anthropogenic EF values are close to

those in American (Cypress Blue, Florida – Kamenov et al., 2009) and European peat records (EGR, Switzerland – Krachler et al., 2003; Black Forest, Germany – Aubert et al., 2006). However the EF of La does not exceed 2.5 even in the Modern period (see upper panel in SM2).

Using the UCC as a natural reference we calculated the detrital fraction of REE in equilibrium with the Sc content in our samples as follows: Detrital REE = $(ratio\ sum\ REE/Sc)_{UCC} \times [Sc]_{sample}$. This detrital component is removed from the measured $[REE]_{samples}$ to estimate the excess, mainly anthropogenic, REE contribution. Some anthropogenic contribution is detected since the Roman Period, but the enrichment in all REE is only obvious since the Industrial Revolution. Fig. 4 shows for instance, the total (i.e., natural + anthropogenic) and anthropogenic fluxes for La, Nd and sum REE. The relationship between Pb content and Pb isotopic data (Fig. 3b) confirms the significant human influence in the Misten trace metal record over the last 3 centuries.

4.3. Source of dust

REE abundance and LREE/HREE fractionation are used to discriminate the sources of dust (Fig. 5). We report

Table 2a
Nd isotopic data and eNd.

Depth cm	$^{143}\text{Nd}/^{144}\text{Nd}$	$\pm 2\text{se}$	eNd	Mode	Run
2.2	0.512123	0.000015	-10.1	Dry	30 10 2009
10.1	0.512119	0.000018	-10.1	Dry	30 10 2009
11.9	0.512048	0.000012	-11.5	Dry	30 10 2009
13.7	0.512046	0.000009	-11.6	Dry	30 10 2009
<i>13.7R</i>	<i>0.512047</i>	<i>0.000017</i>	<i>-11.5</i>	<i>Wet</i>	<i>03 11 2009</i>
17.3	0.512018	0.000010	-12.1	Dry	30 10 2009
<i>17.3R</i>	<i>0.512039</i>	<i>0.000018</i>	<i>-11.7</i>	<i>Wet</i>	<i>03 11 2009</i>
19.1	0.512058	0.000010	-11.3	Dry	30 10 2009
<i>19.1R</i>	<i>0.512086</i>	<i>0.000016</i>	<i>-10.8</i>	<i>Wet</i>	<i>3 11 2009</i>
22.7	0.512073	0.000008	-11.0	Dry	30 10 2009
23.6	0.512066	0.000018	-11.2	Dry	30 10 2009
25.6	0.512009	0.000013	-12.3	Dry	30 10 2009
28.6	0.511988	0.000017	-12.7	Dry	30 10 2009
30.6	0.512019	0.000016	-12.1	Dry	30 10 2009
<i>30.6R</i>	<i>0.512003</i>	<i>0.000026</i>	<i>-12.4</i>	<i>Wet</i>	<i>03 11 2009</i>
32.6	0.511995	0.000011	-12.5	Dry	10 08 2011
<u>32.6D</u>	<u>0.511984</u>	<u>0.003</u>	<u>-12.8</u>	<u>Dry</u>	<u>10 08 2011</u>
40.6	0.512034	0.000012	-11.8	Dry	30 10 2009
50.6	0.511993	0.000015	-12.6	Dry	30 10 2009
52.6	0.512020	0.000013	-12.1	Dry	10 08 2011
56.7	0.511972	0.000009	-13.0	Dry	10 08 2011
<u>56.7D</u>	<u>0.511964</u>	<u>0.002</u>	<u>-13.1</u>	<u>Dry</u>	<u>10 08 2011</u>
61.1	0.512002	0.000008	-12.4	Dry	10 08 2011
65.5	0.512039	0.000010	-11.7	Dry	30 10 2009
69.9	0.512039	0.000012	-11.7	Dry	30 10 2009
76.5	0.512055	0.000030	-11.4	Dry	30 10 2009
78.7	0.512049	0.000020	-11.5	Dry	30 10 2009
83.1	0.512033	0.000012	-11.8	Dry	30 10 2009
87.5	0.512016	0.000011	-12.1	Dry	30 10 2009
108.2	0.511997	0.000010	-12.5	Dry	10 08 2011
109.7	0.512020	0.000012	-12.1	Dry	30 10 2009
120.3	0.512042	0.000013	-11.6	Dry	30 10 2009
130.9	0.512044	0.000014	-11.6	Dry	30 10 2009
134	0.512067	0.000009	-11.1	Dry	30 10 2009
<i>135</i>	<i>0.512046</i>	<i>0.000020</i>	<i>-11.5</i>	<i>Dry</i>	30 10 2009
<i>138</i>	<i>0.512110</i>	<i>0.000032</i>	<i>-10.3</i>	<i>Dry</i>	30 10 2009
145.6	0.512061	0.000020	-11.3	Dry	30 10 2009
169.9	0.512063	0.000021	-11.2	Dry	30 10 2009

Samples have been analysed in dry mode, replicate (in italics) in wet mode.
Underlined values correspond to duplicates.

for each Misten peat samples their REE content (i.e., sum REE normalized to Sc to take into account any dilution effect) and their LREE/HREE fractionation (i.e., La_N/Yb_N). Two trends are obvious in Fig. 5: the peat samples are either enriched in REE (high sum REE/Sc) or displayed a fractionation between LREE and HREE (high LREE/HREE ratio). Moreover the distribution is controlled by the age of the samples. We will discuss the scattering of the peat Misten data successively for the samples of the pre-Industrial Revolution samples (1), the Industrial Revolution (2) and, the Modern Period (3).

- (1) For most of the pre-Industrial Revolution samples, the ratios of the sum REE/Sc range between 10 and 25, with no LREE/HREE fractionation ($1 < \text{EF} < 1.5$ – Fig. 5). A similar range of Sc-normalised REE content is observed between the European soils (data from European soil geochemical atlas – <http://www.gtk.fi/publ/foregsatlas/>) and the Saharan

airbornes (Moreno et al., 2006): it therefore characterizes the range for natural, regional and distal dust sources.

- (2) During the Industrial Revolution, the Misten samples are enriched in REE (Fig. 2), even when normalized to Sc (Fig. 5). All Industrial Revolution samples (except one) present a sum REE/Sc ratio higher than 25, with no fractionation between La and Yb (Fig. 5). Those samples show a progressive increase in REE, reaching a maximum sum REE/Sc ratio (~50) in the sample found at 1937 AD, at the end of the Industrial Revolution interval (Table 1a). Such REE enrichment is explained by intensive coal combustion over this time interval, coals being characterized by a global REE enrichment (e.g., American coals – Vouk and Piver, 1983). Indeed the Misten samples point towards the average ratio of three main Belgian coal ores (mean sum REE/Sc = 120). When comparing the REE pattern of the

Table 2b
Pb isotopic data and Pb content.

Depth cm	Pb isotope ratios										[Pb]
	208/204	±2se	207/204	±2se	206/204	±2se	208/206	±2se	206/207	±2se	ppm
2.2*	38.0051	0.0025	15.6364	0.0010	18.2913	0.0011	2.07783	0.00004	1.16977	0.00001	10.2
6.5*	37.8913	0.0022	15.6251	0.0009	18.1861	0.0010	2.08356	0.00003	1.16388	0.00001	16.9
10.1*	37.8792	0.0020	15.6046	0.0008	18.0182	0.0009	2.10232	0.00004	1.15466	0.00001	34.6
11.9*	37.8885	0.0012	15.5922	0.0004	17.9503	0.0004	2.11073	0.00005	1.15125	0.00001	179
13.7*	37.8952	0.0022	15.5935	0.0009	17.9533	0.0011	2.11075	0.00004	1.15133	0.00001	265
17.3*	37.7040	0.0039	15.5872	0.0017	17.8752	0.0019	2.10931	0.00004	1.14679	0.00002	339
19.1*	37.9916	0.0021	15.5998	0.0007	18.0246	0.0008	2.10773	0.00004	1.15546	0.00001	622
22.7*	38.2254	0.0020	15.6153	0.0008	18.2379	0.0009	2.09592	0.00004	1.16796	0.00001	591
23.6*	38.1925	0.0015	15.6147	0.0006	18.2011	0.0007	2.09841	0.00005	1.16564	0.00001	489
25.6*	38.2856	0.0021	15.6180	0.0008	18.3017	0.0009	2.09192	0.00004	1.17183	0.00001	175
28.6*	38.3457	0.0022	15.6209	0.0008	18.3662	0.0009	2.08791	0.00005	1.17571	0.00001	118
30.6*	38.3582	0.0019	15.6178	0.0008	18.3840	0.0010	2.08651	0.00004	1.17711	0.00001	63.1
40.6	38.3777	0.0023	15.6215	0.0008	18.3973	0.0008	2.08609	0.00004	1.17768	0.00001	36.9
50.6	38.3785	0.0018	15.6247	0.0007	18.3900	0.0007	2.08692	0.00003	1.17697	0.00001	15.6
56.7	38.3561	0.0022	15.6237	0.0010	18.3844	0.0011	2.08638	0.00004	1.17668	0.00001	11.7
65.5	38.3965	0.0020	15.6277	0.0008	18.4251	0.0009	2.08393	0.00004	1.17898	0.00001	4.19
69.9	38.4866	0.0019	15.6353	0.0008	18.5058	0.0009	2.07972	0.00004	1.18359	0.00001	2.53
76.5	38.5652	0.0018	15.6442	0.0008	18.5708	0.0009	2.07669	0.00005	1.18708	0.00001	1.52
78.7	38.5476	0.0033	15.6399	0.0014	18.5650	0.0016	2.07636	0.00004	1.18703	0.00001	1.31
83.1	38.6112	0.0023	15.6473	0.0009	18.6164	0.0010	2.07407	0.00004	1.18974	0.00001	1.39
87.5	38.5753	0.0024	15.6411	0.0009	18.5909	0.0011	2.07498	0.00005	1.18859	0.00002	1.04
109.7	38.2657	0.0024	15.6109	0.0008	18.3112	0.0010	2.08975	0.00004	1.17297	0.00001	14.2
120.3	38.3471	0.0018	15.6168	0.0008	18.3852	0.0009	2.08582	0.00004	1.17727	0.00001	34.4
130.9	38.3694	0.0019	15.6239	0.0007	18.3873	0.0007	2.08672	0.00004	1.17687	0.00001	54.5
134.0	38.3684	0.0026	15.6236	0.0009	18.3851	0.0010	2.08691	0.00004	1.17678	0.00001	61.4
135.0	38.2948	0.0021	15.6165	0.0008	18.3241	0.0008	2.08990	0.00004	1.17337	0.00001	59.5
138.1	38.3719	0.0023	15.6232	0.0009	18.3865	0.0009	2.08699	0.00004	1.17686	0.00001	47.9
145.6	38.3716	0.0020	15.6219	0.0008	18.3886	0.0009	2.08666	0.00004	1.17713	0.00001	15.2
169.9	38.5086	0.0019	15.6394	0.0008	18.4658	0.0009	2.08538	0.00005	1.18073	0.00001	2.84

Samples have been analysed in dry mode, replicate (in italics) in wet mode.

Pb content data are from [Allan et al. \(2013b\)](#).

* Indicates isotopic data already published ([Allan et al., 2013b](#)).

Misten samples with the available REE signature of some of the important pollution sources in Europe, the samples characterized by the highest REE content and EF were close to the mean signatures of Belgian coals (Fig. 2).

- (3) In contrast, the Modern Period samples are characterized by a shift in their La_N/Yb_N ratios (up to 2.5) without marked enrichment in REE (Fig. 5). The distribution of the Modern Period peat samples rather suggest another anthropogenic REE source. For instance, steel plant dust collected from an urban European area (close to the France–Germany border, [Geagea et al., 2007](#)) exhibits a marked enrichment in La ($La_N/Yb_N = 3.7$, Table 1a, Fig. 5) but only a slight enrichment in REE (Fig. 2). Steel plant dust could be a potential candidate to explain the observed REE fractionation in the Misten samples over the Modern Period.

For the Industrial Revolution and the Modern period, our REE data confirm the shift in Pb isotope ratios already observed by [Allan et al. \(2013a\)](#) in the upper Misten peat record (Fig. 3a and b). Based on trace metal elements and Pb isotope data they concluded that coal and metallurgy,

in particular the exploitation of regional Pb–Zn ores, were the main pollutant activities over the past 300 years. In Belgium, anthropogenic dust was mainly derived from pre-1945 non-ferrous mining and refining ([Schmitz, 1979](#); [Dejonghe, 1998](#)). The high dust contamination by coal combustion at AD 1937 is in agreement with the maximum Belgian coal production (1927–1955 AD in [Rutledge, 2011](#)) and with the historical pollution record in North European bogs (1930–1970 in [Shoty et al., 2003](#)). It is likely that the presence of anthropogenic derived-REE in the environment (which strongly increased between 1950 and 2000) is due to their use in industry, medicine, and agriculture ([Geagea et al., 2007](#)).

Although we record an REE enrichment in the upper peat layers, no obvious influence of anthropogenic activities is observed in the Nd isotope Misten dataset for both the Roman period and the Middle Ages, the range of Nd isotope ratios being similar with the scattering of the natural dust sources (Fig. 3a and b, Table 3). We conclude therefore, that at least before the Industrial Revolution, the Nd isotope variations are mainly due to changes in relative proportion of regional and distal sources. In contrast, an influence of gasoline and then diesel soot may explain the shift towards less negative ϵNd values (from -12 to

Table 3
Synthesis of Nd and Pb signature for natural and anthropogenic dust sources.

Source	Sample location	206/207	eNd	References
<i>Natural dust sources</i>				
Upper Continental Crust	Worldwide mean	1.205		Millot et al. (2004)
European variscan crust	<i>Mean</i>	<i>1.199</i>	<i>-10.8</i>	Michard et al. (1985)
European variscan crust	<i>Median</i>	<i>1.200</i>	<i>-10.9</i>	Michard et al. (1985)
European loess	Belgium k14		-12.6	Grousset et al. (1988a,b)
European loess	Belgium r11		-12.0	Grousset et al. (1988a,b)
European loess	France PR		-10.9	Grousset et al. (1988a,b)
European loess	France hot		-10.7	Grousset et al. (1988)
European loess	France ns 6		-10.8	Grousset et al. (1988a,b)
European loess	France hc90/1		-12.5	Grousset et al. (1988a,b)
European loess	UK scil		-11.7	Grousset et al. (1988a,b)
<i>European loess</i>	<i>Mean</i>		<i>-11.6</i>	
Saharan aerosols	East Atlantic Ocean		-14.2	Grousset et al. (1988a,b)
Saharan aerosols	East Atlantic Ocean		-12.8	Grousset et al. (1988a,b)
Saharan aerosols	East Atlantic Ocean		-12.7	Grousset et al. (1988a,b)
Saharan aerosols	East Atlantic Ocean		-13.9	Grousset et al. (1988a,b)
Saharan aerosols	East Atlantic Ocean		-12.7	Grousset et al. (1988a,b)
Saharan aerosols	East Atlantic Ocean		-12.7	Grousset et al. (1988a,b)
Saharan aerosols	East Atlantic Ocean		-11.2	Grousset et al. (1988a,b)
Saharan aerosols	JL-46		-13.6	Goldstein et al. (1984)
Saharan aerosols	JL-48		-12.1	Goldstein et al. (1984)
Saharan aerosols	Off cape verde		-11.2	Rognon et al. (1996)
Saharan aerosols	Off cape verde		-12.8	Rognon et al. (1996)
Saharan aerosols	Corsica		-11.3	Colin (1993)
Saharan aerosols	Corsica		-13.2	Colin (1993)
Saharan aerosols	Corsica		-14.1	Colin (1993)
Saharan aerosols	Corsica		-14.6	Colin (1993)
Saharan aerosols	Corsica		-12.0	Colin (1993)
Saharan aerosols	Canarie		-13.4	Grousset et al. (1988a,b)
Saharan aerosols	Off saint louis		-14.6	Grousset et al. (1988a,b)
Saharan aerosols	Cape verde		-11.2	Grousset et al. (1988a,b)
Saharan aerosols	Niamey		-10.0	Grousset et al. (1988a,b)
Saharan aerosols	Cape verde		-14.4	Grousset et al. (1988a,b)
Saharan aerosols	Cape verde		-12.8	Grousset et al. (1988a,b)
Atmospheric deposition	Capo cavallo		-14.2	Henry et al. (1994)
<i>Saharan aerosol</i>	<i>Mean (n = 23)</i>		<i>-12.9</i>	
Ice-core dust Antarctica	min	1.200		Vallelonga et al. (2002)
Ice-core dust Antarctica	Max	1.250		Vallelonga et al. (2002)
Early Cambrian shale	Brabant massif		-11.3	André et al. (1986)
Early Cambrian pyllade	Brabant massif		-10.8	Linnemann et al. (2012)
<i>Lower Paleozoic shale</i>	<i>Brabant massif (mean)</i>		<i>-12.2</i>	Data from Linnemann et al. (2012)
<i>Antropogenic sources</i>				
Modern airbornes	Benelux	1.146		Bollhöfer and Rosman (2001)
Pb-Zn ores	Eifel, Germany, max	1.189		Durali-Mueller et al. (2007)
Pb-Zn ores	Eifel, Germany, min	1.149		Durali-Mueller et al. (2007)
Pb-Zn ores	Belgium, max	1.188		Cauet and Herbosh (1982) and Dejonghe (1998)
Pb-Zn ores	Belgium, min	1.167		Cauet and Herbosh (1982) and Dejonghe (1998)
Steel plant	Filter dust Rhine valley	1.154	-17.5	Geagea et al. (2007)
Steel plant	Filter dust Rhine valley	1.151	-17.5	Geagea et al. (2008a)
Car soot	Diesel	1.160	-6.0	Geagea et al. (2008a)
Car soot	Unlead gasoline	1.090	-6.9	Geagea et al. (2008a)
Urban airbornes	Rhine valley (Kehl)	1.155	-15.7	Geagea et al. (2008a)
Urban airbornes	Rhine valley (Lokh)	1.150	-5.7	Geagea et al. (2008a)
Urban airbornes	Rhine valley (Lokh)	1.149	-6.5	Geagea et al. (2008a)

Calculated mean values from literature data are reported in italics.

-10) observed for the Modern period samples. In the further climate-related interpretation of the Nd isotope signal we will not discuss the changes over the past 50 years and we will be cautious for the changes observed during the Industrial Revolution.

4.4. Climate-related dust record in Misten peat bog over the historical period

We propose here to integrate elemental and isotopic geochemical data to track potential climatic influences on

the ombrotrophic peatland. In order to decipher the climate signal in the dust deposition in the Misten bog we first utilise major and trace elements to derive the total dust deposition. Second, for each dust-rich identified interval we compare the Nd isotope composition with the local, regional or distal sources to identify the dominant natural atmospheric supplies. Third, we interpret the changes of sources in terms of local or global environmental changes.

Recently, the combination of elemental and isotopic Nd geochemical data has been successfully applied in Holocene ombrotrophic peat profile from Switzerland to quantify the dust deposition, to identify the sources of dust and to provide evidence of climate–dust interactions (Le Roux et al., 2012). Here the approach is applied but focused in on the historical period, an interval characterised by significant environmental perturbations due to human industrial activities.

The dust flux was calculated according to Shotyk et al. (1998) but we use either the sum of REE or the Ti content as the conservative element to calculate the Ti or the REE accumulation rate (AR) over the past 2500 years:

$$\text{Dust fluxes calculated from element X, expressed in } \text{g m}^{-2} \text{y}^{-1} \\ = \text{AR}_X / [X]_{\text{UCC}}$$

where X = Ti or sum REE, UCC = Upper Continental Crust (Ti = 4100 ppm; sum REE = 146.4 $\mu\text{g g}^{-1}$ – data from McLennan, 2001).

Both elements give similar dust flux profiles, confirming the conservative behaviour of REE (Fig. 6). The Ti-calculated fluxes range between 0.5 and 5 $\text{g m}^{-2} \text{y}^{-1}$ for more than 2000 years then increase up to 10 $\text{g m}^{-2} \text{y}^{-1}$ at the beginning of the Industrial Revolution period (sample at 25 cm, 1788 AD). A second significant increase is observed over the past 50 years, the Ti-derived dust flux being multiplied by a factor of two between 1953 AD (7.4 $\text{g m}^{-2} \text{y}^{-1}$ at 20 cm) and 1990 AD (17 $\text{g m}^{-2} \text{y}^{-1}$ at 15 cm). This recent trend records the dominant anthropogenic source of dust deposition (including REE) in the upper 20 cm of the Misten bog.

A close-up view shows evidence of the existence of five intervals. The first interval covers most of the Roman period: it is characterised by a low dust flux, except for an increase around 300 BC. The following four intervals (600 AD, 1000 AD, 1200 AD and from 1700 AD) are characterized by an increase in dust fluxes, recording either the influence of human activities related to land use change (regional erosion due to forest clearance and soil cultivation activities) or to local or regional climate changes (humidity, temperature, wind strength). Recent studies performed on

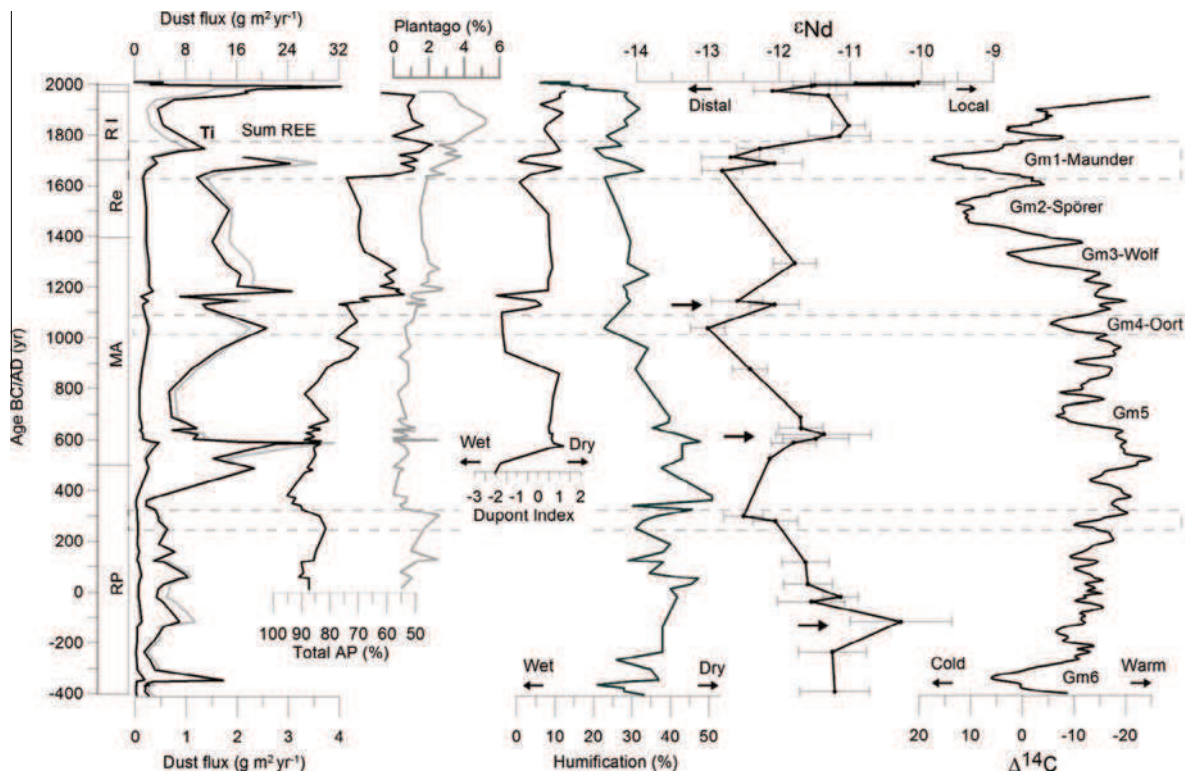


Fig. 6. Evolution of Ti-dust flux, sum REE-dust flux, abundance of arbustive (tree and shrub) pollen, changes in macrofossil assemblages (expressed as Dupont index, Dupont, 1986), peat humification degree and Nd isotope composition (expressed as ϵNd) measured in the Misten bog over the past 2500 years. Pollen and macrofossil data are from Streef et al. (2014) and De Vleeschouwer et al. (2010), respectively. The changes of radiocarbon cosmogenic production (data from Reimer et al., 2009) represent the global climate conditions, with more radiocarbon production during colder intervals. The grand minima of solar activity are reported from Usoskin et al. (2007). The dash boxes underline the distal-rich intervals corresponding to cold event. The arrows indicate intervals characterised by dominant local sources. See text for explanation.

the upper 1 m of several Misten peat cores emphasize the last millennium changes in vegetation, organic and/or inorganic geochemistry mainly recorded human perturbations (De Vleeschouwer et al., 2009, 2012, Allan et al., 2013a,b).

The climate interpretation of major and trace elements in ombrotrophic peat thus requires an additional proxy, here the Nd isotope signature, to distinguish between higher dust fluxes related to enhanced local erosion (mainly anthropogenic influence related to land use change) and higher dust fluxes related to enhanced distal supplies (mainly climatic influence). We use the Nd isotope signature of peat to decipher between local and distal sources (such as in Le Roux et al., 2012). The observed ϵNd variability (-13 to -9) in Misten peat samples is interpreted as a mixing between dust sources (Table 3) from local (Early Cambrian shales = -11.3 , André et al., 1986; Early Cambrian phyllades = -10.8 and mean Paleozoic shales = -12.2 , Linnemann et al., 2012), regional soils (mean European crust = -10.8 , Michard et al., 1985; mean European loess = -11.6 , data from Gallet et al., 1998) and desert particles (mean Saharan airbornes = -12.9 – data from Goldstein et al., 1984; Grousset et al., 1988a,b; Colin, 1993; Henry et al., 1994; Rognon et al., 1996). The ϵNd variability is further compared with the humification degree to evaluate the local relative humidity conditions (Fig. 6). The Sum REE/Sc ratio is used as a complementary proxy to confirm the origin, (local/regional or distal) of the dust (see SM3).

- (1) For most of the Roman period the ϵNd values (mean -11.2), the dust flux ($0.9 \text{ g m}^{-2} \text{ y}^{-1}$ calculated from the sum REE) and the humification degree (HD $\sim 40\%$) remain stable. The range of ϵNd values is consistent with the signature of local soils (mean European crust = -10.8 , mean European loess = -11.6). Note the local origin of the dust is also supported by the relatively low sum REE/Sc ratios (< 23) for most of the Roman period (see SM3). For most of this first interval the relatively dry conditions (high HD) promote the erosion of local soils. The end of the Roman period is then characterized by a change in dust supplies. We observe a decrease of the ϵNd to -12.2 around 300 AD and an increase of the sum REE/Sc ratio ≥ 25 around 120 AD (see SM3). Those changes are not related to any significant increase in dust, so they may be explained by relatively greater supplies from distal sources (i.e., Saharan airbornes), with local conditions being slightly wetter.
- (2) The transition between the Roman period and the Middle Ages (400–600 AD) is marked by less negative ϵNd values and low sum REE/Sc ratios. The higher dust flux reflects more local erosion partly related to drier conditions; the degree of humification reaches its highest value (50%) within this interval. This interval is also marked by a slight decrease in arboreal pollen abundance. The low abundance of pollen indicative of agricultural (e.g., cereal pollen remain below 2% – Streele et al., 2014) suggests that the changes in dust supplies are driven by climate changes.

- (3) The ϵNd data then shift again to more negative values (-13 at 1015 AD). The sum REE/Sc ratio also displays relatively high values (20–21 – see SM3). The higher dust flux records more distal supplies, the local erosion being reduced by the wetter soil conditions, as underlined by a short decrease of the degree of humification plus a change in the plant macroremain assemblages (De Vleeschouwer et al., 2010). We observe that the less negative ϵNd values, the highest dust flux and the low humification values occur within the Oort solar minima event (Fig. 6). For the Misten bog, a similar relationship between solar activity and dust flux was already suggested by De Vleeschouwer et al. (2012). The potential link between enhanced distal supplies and cold climate requires further investigation as little is known about the influence of a global colder climate event on Saharan airborne particle production and transport.
- (4) The following increase in dust flux (at 45–47 cm, 1200–1174 AD) occurs during the Medieval Warm Period before the next cold event (Wolf solar minimum). More local erosion may be partly explained by drier conditions as evidenced by a brief increase in the degree of humification. Note that this change in local soil conditions is also sustained by drier plant macrofossil assemblages (De Vleeschouwer et al., 2010). The sharp increase in dust is probably also influenced by a major change in vegetation cover. Indeed this interval is marked by a sharp decrease in arboreal pollen abundance since 1150 AD (Fig. 6), most likely due to human-induced forest clearance for agriculture purposes (Streele et al., 2014). It coincides with a significant increase in cerealia and *Plantago* pollen, two pollen types that are directly related to farming activity. Since such land-use change enhances local erosion, the higher dust flux is therefore explained by both drier local conditions and human-controlled change in vegetal cover.
- (5) The ϵNd return again to more negative values (-13) at the end of the Renaissance period (1691 AD at 30 cm). This shift coincides with high sum REE/Sc ratio (i.e., 25 around 1600 AD). The humification degree is variable during this interval, with on average wetter conditions. The enhanced distal-dust flux would reflect the global colder climate during the Maunder solar minimum (similar to point 3).

After the Maunder minimum the ϵNd becomes less negative, recording again more local dust supplies. Even this shift occurs during the post-Little Ice Age warming, the climate forcing is not obvious as coal combustion delivers a significant REE contribution during the Industrial Revolution (Fig. 5). Such anthropogenic sources bring no peculiar Nd isotope signature as the coal-derived dusts have a crustal fingerprint similar (see reported REE patterns at Fig. 3) with the local sources.

5. CONCLUSION

Our results provide evidence that climate forcing may be detected in ombrotrophic peat, even for the historical period that is characterised by a mixed climate-human control. The Misten geochemical dataset emphasizes a significant anthropogenic REE contribution, first by coal combustion during the Industrial Revolution and then by industrial activities for the Modern Period. Before the Industrial Revolution, the REE abundance ($10 < \text{sumREE}/\text{Sc} < 25$) and ϵNd variability (-13 to -9) in peat is interpreted by a mixing between dust sources from local soils and distal desert particles. Dominant local dust supplies (at ca. 100 AD, 600 AD and 1200 AD) systematically occur during drier (higher humification) intervals, the erosion of surrounding soils being promoted by the local environmental conditions. In contrast, the three periods characterised by dominant-distal sources (at ca. 320 AD, 1000 AD and 1700 AD) are consistent with local wetter intervals as indicated by their lower degree of humification. Since local erosion is reduced, the site is more sensitive to distal supplies. On a global scale, two of those distal-rich intervals (ca. 1000 AD and 1700 AD) occur during cold events, in particular during the Oort and Maunder minima. Such observations may suggest that cold climate would favour distal desert supplies, a hypothesis requiring further validation in other settings.

ACKNOWLEDGEMENTS

We thank all the persons who contribute to this work and especially Maurice Strel from ULg (coring agreement), William Shotyk for the Ti-Wardenaar corer, and the use of the peat lab facilities at Heidelberg; François De Vleeschouwer from Ecolab (coring); Mona-Court Picon from Royal Institute for Natural Sciences in Brussels (coring and sub-sampling); Frederic Candaudap and Aurélie Lanzaova from Observatoire Midi-Pyrénées (ICP-MS analyses), Ivan Petrov and Jeroen de Jong at ULB (MC-ICP-MS analyses). We also acknowledge Camille Delvigne at ULB who accepts to share her master's thesis data from Belgian coals. The manuscript has been improved by the constructive comments of three reviewers and by the editor, prof. D. Weiss. The English has been kindly improved by Prof. Shaun Lovejoy (McGill, Montreal) and Anson Mackay (UCL, London). This study was funded by the Walloon Region and the FNRS.

APPENDIX A. SUPPLEMENTARY DATA

Supplementary data associated with this article can be found, in the online version, at <http://dx.doi.org/10.1016/j.gca.2014.03.014>.

REFERENCE

- André L., Deutsch S. and Hertogen J. (1986) Trace-element and Nd isotopes in shales as indexes of provenance and crustal growth: the early Paleozoic from the Brabant Massif (Belgium). *Chem. Geol.* **57**, 101–115.
- Allan M., Le Roux G., Sonke J. E., De Vleeschouwer F., Piotrowska N., Sikorski J., Strel M. and Fagel N. (2013a) Historical record of atmospheric mercury deposition in Western Europe: the Misten peat bog (Hautes Fagnes – Belgium). *Sci. Total Environ.* **442**, 290–301.
- Allan M., Le Roux G., De Vleeschouwer F., Bindler R. and Fagel N. (2013b) High-resolution reconstruction of atmospheric deposition of trace metals and metalloids since 300 years in Belgium recorded by ombrotrophic peat cores (Hautes-Fagnes, Belgium). *Environ. Pollut.* **178**, 1–14.
- Allan M., Le Roux G., Piotrowska N., Beghin J., Javaux E., Court-Picon M., Mattielli N., Verheyden S. and Fagel N. (2013c) Mid and late Holocene dust deposition in western Europe: the Misten peat bog (Hautes Fagnes – Belgium). *Clim. Past Discuss.* **9**, 2889–2928. <http://dx.doi.org/10.5194/cpd-9-2889-2013>.
- Anshari G., Kershaw A. P. and van der Kaars S. (2001) A late pleistocene and holocene pollen and charcoal record from peat swamp forest, lake sentarum wildlife Reserve, West Kalimantan, Indonesia. *Palaeogeogr. Palaeoclim. Palaeoecol.* **171**, 213–228.
- Aubert D., Le Roux G., Krachler M., Cheburkin A., Kober B., Shotyk W. and Stille P. (2006) Origin and fluxes of atmospheric REE entering an ombrotrophic peat bog in Black Forest (SW Germany): Evidence from snow, lichens and mosses. *Geochim. Cosmochim. Acta* **70**, 2815–2826.
- Blaauw M. and Christen J. A. (2011) Flexible paleoclimate age-depth models using an autoregressive gamma process. *Bayesian Anal.* **6**, 457–474.
- Barber K. E., Chambers F. M. and Maddy D. (2003) Holocene palaeoclimates from peat stratigraphy: macrofossil proxy climate records from three oceanic raised bogs in England and Ireland. *Quatern. Sci. Rev.* **22**, 521–539.
- Belokopytov I. E. and Veresnevich V. V. (1955) Giktorf's peat borers. *Torfânaâ Promyslennost* **8**, 9–10.
- Bradley R. S. (1999) *Paleoclimatology. Reconstructing climates of the Quaternary*. Second edition. International Geophysics Series 64, Academic Press, San Diego, pp. 613.
- Björck S. and Clemmensen L. B. (2004) Aeolian sediment in raised bog deposits, Halland, SW Sweden: a new proxy record of Holocene winter storminess variation in southern Scandinavia. *Holocene* **14**, 677–688.
- Bollhöfer A. and Rosman K. J. R. (2001) Isotopic source signatures for atmospheric lead: the Northern Hemisphere. *Geochim. Cosmochim. Acta* **65**, 1727–1740.
- Bourginon P. (1953) Associations minéralogiques des limons et argiles des hautes-Fagnes. *Ann. Soc. Geol. Belg.* **77B**, 39–59.
- Cauet S. W. D. and Herbosh A. (1982) Genetic study of Belgian lead zinc mineralizations in carbonate environments through lead isotope geochemistry. *Bull. BRGM* **3**, 29–41.
- Chambers F. M., Booth R. K., De Vleeschouwer F., Lamentowicz M., Le Roux G., Mauquoy D., Nichols J. E. and van Geel B. (2012) Development and refinement of proxy-climate indicators from peats. *Quatern. Int.* **268**, 21–33.
- Chambers F. M., Beilman D. W. and Zicheng Yu. (2011) Methods for determining peat humification and for quantifying peat bulk density, organic matter and carbon content for palaeostudies of climate and peatland carbon dynamics. *Mires Peat* **7**, 1–10.
- Chambers F. M. and Charman D. J. (2004) Holocene environmental change: contributions from the peatland archive. *Holocene* **14**, 1–6.
- Charman D. and Mäkilä M. (2003) Climate reconstruction from peatlands. *PAGES Newslitt.* **11**, 15–17.
- Chauvel C. and Blichert-Toft J. (2001) A hafnium isotope and trace element perspective on melting of the depleted mantle. *Earth Planet. Sci. Lett.* **190**, 137–151.
- Clymo R. S. (1987) The ecology of peatlands. *Sci. Prog.* **71**, 593–614, Oxford.

- Colin C. (1993) Etude isotopique des retombées atmosphériques-totales en Méditerranée occidentale. DEA Université Paris XI.
- Davis B. A. S., Brewer S., Stevenson A. C. and Guiot J. (2003) The temperature of Europe during the Holocene reconstructed from pollen data. *Quatern. Sci. Rev.* **22**, 1701–1716.
- Dejonghe L. (1998) Zinc-lead deposits of Belgium. *Ore Geol. Rev.* **12**, 329–354.
- D'Almeida G. A. (1986) A model for saharan dust transport. *J. Clim. Appl. Meteorol.* **25**, 903–916.
- De Vleeschouwer F., Gérard L., Goormaghtigh C., Mattielli N., Le Roux G. and Fagel N. (2007) Atmospheric lead and heavy metal pollution records from a Belgian peat bog spanning the last two millennia: Human impact on a regional to global scale. *Sci. Total Environ.* **377**, 282–295.
- De Vleeschouwer F., Piotrowska N., Sikorovsky J., Pawlyta J., Cheburkin A. K., Le Roux G., Lamentowicz M., Fagel N. and Mauquoy D. (2009) A ca. 1300-year multiproxy record of palaeoenvironmental changes in an ombrotrophic peat bog from northern Poland. *Holocene* **19**, 625–637.
- De Vleeschouwer F., Luthers, C. and Strel, M. et al. (2010) Recherche d'intérêt général et pluridisciplinaire relative aux modalités de l'accumulation récente de la tourbe dans la tourbière ombrogène du Misten (Hautes-Fagnes) en relation avec les changements climatiques et les effets des activités humaines. La Cellule Etat de l'environnement wallon. pp. 98. Available from: <<http://etat.environnement.wallonie.be/index.php?page=etudes-detaillees>> (In French).
- De Vleeschouwer F., Pazdur A., Luthers C., Strel M., Mauquoy D. and Wastiaux C., et al. (2012) A millennial record of environment change in peat deposit from the Misten (East Belgium). *Quat. Int.* <http://dx.doi.org/10.1016/j.quaint.2011.12.010>.
- Dunlap C. E., Steinnes E. and Flegal A. R. (1999) A synthesis of lead isotopes in two millennia of European air. *Earth Planet. Sci. Lett.* **167**, 81–88.
- Dupont L. M. (1986) Temperature and rainfall variation in the Holocene based on comparative palaeoecology and isotope geology of a hummock and a hollow (Bourtangerveen, The Netherlands). *Rev. Palaeobot Palynol.* **48**, 71–159.
- Durali-Mueller S., Brey G. P., Wigg-Wolf D. and Lahaye Y. (2007) Roman lead mining in Germany: its origin and development through time deduced from lead isotope provenance studies. *J. Archaeol. Sci.* **34**, 1555–1567.
- Engelstaedter S. and Washington R. (2007) Atmospheric controls on the annual cycle of North African dust. *J. Geophys. Res.* **112**, D03103.
- Ferrat M., Weiss D. J., Dong S., Large D. J., Spiro B., Sun Y. and Gallagher K. (2012a) Lead atmospheric deposition rates and isotopic trends in Asian dust during the last 9.5 kyr recorded in an ombrotrophic peat bog on the eastern Qinghai-Tibetan Plateau. *Geochim. Cosmochim. Acta* **82**, 4–22.
- Ferrat M., Weiss D. J. and Strekopytov S. (2012b) A single procedure for the accurate and precise quantification of the rare earth elements, Sc, Y, Th and Pb in dust and peat for provenance tracing in climate and environmental studies. *Talanta* **93**, 415–423.
- Finsinger W., Tinner W., van der Knaap W. O. and Ammann B. (2006) The expansion of hazel (*Corylus avellana* L.) in the southern Alps: a key for understanding its early Holocene history in Europe? *Q. Sci. Rev.* **25**, 612–631.
- Frankard P., Ghiette P., Hindryckx M.-N., Schumacker R. and Wastiaux C. (1998) Peatlands of Wallony (S-Belgium). *Suo* **49**, 33–47.
- Gaida R., Olbrechts S., Hindrinckx M.-N., Schumacker R. and Radtke U. (1997) Elementverteilung in einem Moorprofil (Präboreale bis Subatlantikum) im tal der Helle/Hill (Hohes Venn, Belgien). *Geoökodynamik* **28**, 79–90.
- Gaida R., Schumacker R., Sauer K. H. and Radtke U. (1993) Elementverteilung in einem Moorprofil aus dem Mittel- und JungHolozän (Atlantikum bis Subatlantikum) im Wallonischen Venn (Hohes Venn, Belgien). *Düsseldorfer Geograph. Schriftenr.* **31**, 117–140.
- Galer S. J. G. and Abouchami W. (1998) Practical application of lead triple spiking for correction of instrumental mass discrimination. 8th Goldschmidt Conf. *Min. Mag.* **62A**, 491–492.
- Gallet S., Jahn B. M., Van Vliet Lanoe B., Dia A. and Rossello E. (1998) Loess geochemistry and its implications for particle origin and composition of the upper continental crust. *Earth Planet. Sci. Lett.* **156**, 157–172.
- Geagea M. L., Stille P., Millet M. and Perrone T. (2007) REE characteristics and Pb, Sr and Nd isotopic compositions of steel plant emissions. *Sci. Total Environ.* **373**, 404–419.
- Geagea M. L., Stille P., Gauthier-Lafaye F. and Millet M. (2008a) Tracing of industrial aerosol sources in an urban environment using Pb, Sr, and Nd Isotopes. *Environ. Sci. Technol.* **42**, 692–698.
- Geagea M. L., Stille P., Gauthier-Lafaye F., Perrone T. and Aubert D. (2008b) Baseline determination of the atmospheric Pb, Sr and Nd isotopic compositions in the Rhine valley, Vosges mountains (France) and the Central Swiss Alps. *Appl. Geochem.* **23**, 1703–1714.
- Givelet N., Le Roux G., Cheburkin A., Chen B., Frank J., Goodsite M., Kempter H., Krachler M., Noernberg T., Rausch N., Rheinberger S., Roos-Barraclough F., Sapkota A., Scholz C. and Shotyck W. (2004) Suggested protocol for collecting, handling and preparing peat cores and peat samples for physical, chemical, mineralogical and isotopic analyses. *J. Environ. Monit.* **6**, 481–492.
- Goldstein R. K., O'Nions and Hamilton P. J. (1984) A Sm–Nd isotopic study of atmospheric dust particulates from major river systems. *Earth Planet. Sci. Lett.* **70**, 221–236.
- Goudie A. S. and Middleton N. J. (2001) Saharan dust storms: nature and conséquences. *Earth Sci. Rev.* **56**, 179–204.
- Grousset F. E., Biscaye P. E., Zindler A., Prospero J. and Chester R. (1988a) Neodymium isotopes as tracers in marine sediments and aerosols: North Atlantic. *Earth Planet. Sci. Lett.* **87**, 367–378.
- Grousset F. E., Parra M., Bory A., Martinez P., Bertrand P., Shimmield G. and Ellam R. M. (1998b) Saharan wind regimes traces by Sr–Nd isotopic composition of subtropical atlantic sediments: last glacial maximum vs today. *Quat. Sci. Rev.* **17**, 395–409.
- Harrison S., Kohfeld K. E., Roelandt C. and Claquin T. (2001) The role of dust in climate changes today, at the last glacial maximum and in the future. *Earth Sci. Rev.* **54**, 43–80.
- Henry F., Jeandel C., Dupré B. and Minster J. F. (1994) Particulate and dissolved Nd in the western Mediterranean Sea: sources, fate and budget. *Mar. Chem.* **45**, 283–305.
- Hong Y. T., Jiang H. B., Liu T. S., Zhou L. P., Beer J., Li H. D., Leng X. T., Hong B. and Qin X. G. (2000) Response of climate to solar forcing recorded in a 6000-year $\delta^{18}\text{O}$ time-series of Chinese peat cellulose. *Holocene* **10**, 1–7.
- Kamenov G. D., Brenner M. and Tucker J. L. (2009) Anthropogenic versus natural control on trace element and Sr–Nd–Pb isotope stratigraphy in peat sediments of southeast Florida (USA), ~1500 AD to present. *Geochim. Cosmochim. Acta* **73**, 3549–3567.
- Kellogg C. A. and Griffin D. W. (2006) Aerobiology and the global transport of desert dust. *Trends Ecol. Evol.* **21**, 638–644.

- Kempton H. (1996) Der Verlauf des anthropogenen elementeintrags in Regenwassermoore des westlichen Mitteleuropas während des jüngeren Holozäns. *Paläoklimaforschung* **26**, 309.
- Klaminder J., Renberg I., Bindler R. and Emteryd O. (2003) Isotopic trends and background fluxes of atmospheric lead in northern Europe: analyses of three ombrotrophic bogs from south Sweden. *Global Biogeochem. Cycles* **17**, 1019.
- Krachler M., Mohl C., Emons H. and Shotyk W. (2002) Analytical procedures for the determination of selected trace elements in peat and plant samples by inductively coupled plasma mass spectrometry. *Spectrochim. Acta Part B: At. Spectrosc.* **57**, 1277–1289.
- Krachler M., Mohl C., Emons H. and Shotyk W. (2003) Two thousand years of atmospheric rare earth element (REE) deposition as revealed by an ombrotrophic peat bog profile, Jura Mountains, Switzerland. *J. Environ. Monit.* **5**, 111–121.
- Kylander M. E., Weiss D. J., Martínez Cortizas A., Spiro B., García-Sánchez R. and Coles B. J. (2005) Refining the pre-industrial atmospheric Pb isotope evolution curve in Europe using an 8000 year old peat core from NW Spain. *Earth Planet. Sci. Lett.* **240**, 467–485.
- Kylander M. E., Bindler R., Martínez Cortizas A., Gallagher K., Mörth C. M. and Rauch S. (2013) A novel geochemical approach to paleorecords of dust deposition and effective humidity: 8500 years of peat accumulation at Store Mosse (the “Great Bog”) Sweden. *Quart. Sci. Rev.* **69**, 69–82.
- Le Roux G., Fagel N., De Vleeschouwer F., Krachler M., Debaille V., Stille P., Mattielli N., Van der Knaap W. O., Van Leeuwen J. F. N. and Shotyk W. (2012) Volcano- and climate-driven changes in atmospheric dust sources and fluxes since the late glacial in Central Europe. *Geology* **40**, 335–338.
- Lambert F., Bigler M., Steffensen J. P., Hutterli M. and Fischer H. (2012) Centennial mineral dust variability in high-resolution ice core data from Dome C, Antarctica. *Clim. Past* **8**, 609–623.
- Lamentowicz M., Obremaska M. and Mitchell E. A. D. (2008) Autogenic succession, land-use change, and climatic influences on the Holocene development of a kettle hole mire in Northern Poland. *Rev. Palaeobot. Palynol.* **151**, 21–40.
- Laurent B., Marticorena B., Bergametti G., Léon J. F. and Mahowald N. M. (2008) Modeling mineral dust emissions from the Sahara desert using new surface properties and soil database. *J. Geophys. Res.* **113**, D14218. <http://dx.doi.org/10.1029/2007JD009484>.
- Lieubeau V., Genthon P., Stievenard M., Nasi R. and Masson-Delmotte V. (2007) Tree-rings and the climate of New Caledonia (SW Pacific): preliminary results from Araucariaceae. *Palaeogeogr. Palaeoclimatol. Palaeoecol.* **253**, 477–489.
- Linnemann U., Herbosch A., Liégeois J.-P., Pin C., Gärtner A. and Hofmann M. (2012) The Cambrian to Devonian odyssey of the Brabant Massif within Avalonia: a review with the new zircon ages, geochemistry, Sm–Nd isotopes, stratigraphy and palaeogeography. *Earth Sci. Rev.* **112**, 126–154.
- McCarthy F. M. G., Collins E. S., Kerr H. A., Scott D. B. and Medioli F. S. (1995) A comparison of postglacial arcellacean (Thecamoebian) and pollen succession in Atlantic Canada, illustrating the potential of arcellaceans for paleoclimatic reconstruction. *J. Paleontol.* **69**, 980–993.
- Martini A. and Martínez-Cortizas A. (2006), Peatlands: basin evolution and depository of records on global environmental and climatic changes. In: *Developments in Earth Surface Processes*, vol. 9. Elsevier, pp. 606.
- Mauquoy D., Engelkes T., Groot M. H. M., Markesteijn F., Oudejans M. G., van der Plicht J. and van Geel B. (2002) High-resolution records of late-Holocene climate change and carbon accumulation in two north-west European ombrotrophic peat bogs. *Palaeogeogr. Palaeoclim. Palaeoecol.* **186**, 275–310.
- Meisel T., Schöner N., Paliulionyte V. and Kahr E. (2002) Determination of rare earth elements, Y, Th, Zr, Hf, Nb and Ta in geological reference materials G-2, G-3, SCO-1 and WGB-1 by sodium peroxide sintering and inductively coupled plasma-mass spectrometry. *Geostand. Newsl.* **26**, 53–61.
- Michard A. P., Gurriet P., Soudaut M. and Albarède F. (1985) Nd isotopes in French Phanerozoic shales: external vs internal aspects of crustal evolution. *Geochim. Cosmochim. Acta* **49**, 601–610.
- Mikova J. and Denkova P. (2007) Modified chromatographic separation scheme for Sr and Nd isotope analysis in geological silicate samples. *J. Geosci.* **52**, 221–226.
- Millot R., Allègre C.-J., Gaillardet J. and Roy S. (2004) Lead isotopic systematics of major river sediments: a new estimate of the Pb isotopic composition of the Upper Continental Crust. *Chemical Geology* **203**(1–2), 75–90.
- Mitchell E. A. D., Charman D. J. and Warner B. G. (2008) Testate amoebae analysis in ecological and paleoecological studies of wetlands: past, present and future. *Biodivers. Conserv.* **17**, 2115–2137. <http://dx.doi.org/10.1007/s10531-007-9221-3>.
- McLennan S. M. (2001) Relationships between the trace element composition of sedimentary rocks and upper continental crust. *Geochem. Geophys. Geosyst.* **2**, 11. <http://dx.doi.org/10.1029/2000GC000109>.
- Moreno T., Castillo S., Alastuey A., Cuevas E., Herrmann L., Mounkaila M., Elvira J. and Gibbons W. (2006) Geochemical variations in aeolian mineral particles from the Sahara-Sahel Dust Corridor. *Chemosphere* **65**, 261–270.
- Moulin C., Guillard F., Dulac F. and Lambert C. E. (1997) Long-term daily monitoring of Saharan dust load over ocean using Meteosat ISCCP-B2 data 1. Methodology and preliminary results for 1983–1994 in the Mediterranean. *J. Geophys. Res.* **102**(D14), 16947–16958.
- Moschen R., Kühl N., Peters S., Vos H. and Lücke A. (2011) Temperature variability at Dürres Maar, Germany during the migration period and at high medieval times, inferred from stable carbon isotopes of Sphagnum cellulose. *Climate Past* **7**, 1011–1026.
- Oppenheimer C. (2003) Climatic, environmental and human consequences of the largest known historic eruption: tambora volcano (Indonesia). *Prog. Phys. Geogr.* **27**, 230–259.
- Payne R. J. (2011) Can testate amoeba-based palaeohydrology be extended to fens? *J. Quatern. Sci.*, **26**, 15–27.
- Persch F. (1950) Zur postglazialen Wald- und Moorentwicklung im Hohen Venn. *Descheniana* **104**, 81–93.
- Piotrowska N. (2013) Status report of AMS sample preparation laboratory at GADAM Centre, Gliwice, Poland. *Nucl. Instrum. Meth. Phys. Res. Sect. B* **294**, 176–181.
- Reimer P. et al. (2009) IntCal09 terrestrial radiocarbon age calibration, 0–26 cal kyr BP. *Radiocarbon* **51**, 1111–1150.
- Renson V., Fagel N., Mattielli N., Nekrasoff S., Streef M. and De Vleeschouwer F. (2008) Roman road pollution assessed by elemental and lead isotope geochemistry in East Belgium. *Appl. Geochem.* **23**, 3253–3266.
- Rognon P., Coudé-Gaussen G., Revel M., Grousset F. E. and Pedemay P. (1996) Holocene Saharan dust deposition on the Cape Verde Islands: sedimentological and Nd–Sr isotopic evidence. *Sedimentology* **43**, 359–366.
- Roos-Barraclough F., van der Knaap W. O., van Leeuwen J. F. N. and Shotyk W. (2004) A Late-glacial and Holocene record of climatic change from a Swiss peat. *Holocene* **14**, 7–19.
- Rutledge D. (2011) Estimating long-term world coal production with logit and probit transforms. *Int. J. Coal Geol.* **85**, 23–31.

- Sapkota A., Cheburkin A. K., Bonani G. and Shotyk W. (2007) Six millennia of atmospheric dust deposition in southern South America (Isla Navarino, Chile). *Holocene* **17**, 561–572.
- Scheuven D., Schutz L., Kandler K., Ebert M. and Winbruch S. (2013) Bulk composition of northern African dust and its source sediments – a compilation. *Earth Sci. Rev.* **116**, 170–194.
- Sikorski J. and Bluszcz A. (2008) Application of α and γ spectrometry in the ^{210}Pb method to model sedimentation in artificial retention reservoir. *Geochronometria* **31**, 65–75. <http://dx.doi.org/10.2478/v10003-008-0019-4>.
- Shotyk W., Weiss D., Appleby P. G., Cheburkin A. K., Frei R. and Gloor M., et al. (1998) History of atmospheric lead deposition since 12,370 ^{14}C yr BP recorded in a peat bog profile, Jura Mountains, Switzerland. *Science* **281**, 1635–1640.
- Shotyk W., Weiss D., Kramers J. D., Frei R., Cheburkin A. K., Gloor M. and Reese S. (2001) Geochemistry of the peat bog at Etang de la Gruère, Jura Mountains, Switzerland, and its record of atmospheric Pb and lithogenic trace metals (Sc, Ti, Y, Zr, and REE) since 12370 ^{14}C yr BP. *Geochim. Cosmochim. Acta* **65**, 2337–2360.
- Shotyk W., Krachler M., Martinez-Cortizas A., Cheburkin A. K. and Emons H. (2002) A peat bog record of natural, pre-anthropogenic enrichments of trace elements in atmospheric aerosols since 12370 ^{14}C yr BP, and their variation with Holocene climate change. *Earth Planet. Sci. Lett.* **199**, 21–37.
- Shotyk W., Goodsite M. E., Roos-Barraclough F., Frei R., Heinemeier J., Asmund G., Lohse C. and Hansen T. C. (2003) Anthropogenic contributions to atmospheric Hg, Pb and As accumulation recorded by peat cores from southern Greenland and Denmark dated using the ^{14}C bomb pulse curve. *Geochim. Cosmochim. Acta* **67**, 3991–4011.
- Schmitz C. (1979) World Non-Ferrous Metal Production and Prices. 1700–1976. Routledge Chapman and Hall.
- Streel M., Beghin J., Gerrienne P., Hindryckx M. N., Luthers C., Court-Picon M., Frankard P., Allan M. and Fagel N. (2014) Late subatlantic history of the ombrotrophic misten bog (Eastern Belgium) based on high resolution pollen, testate amoebae and macrofossil analysis. *Geologica Belgica* **17**(2), 148–160.
- Stuut J. B., Smalley I. and O'Hara-Dhand K. (2009) Aeolian dust in Europe: African sources and European deposits. *Quart. Int.* **198**, 234–245.
- Usoskin I. G., Solanski S. K. and Kovaltsov G. A. (2007) Grand minima and maxima solar activity: new observational constraints. *Astron. Astrophys.* **471**, 301–309.
- Vallelonga P., Van de Velde K., Candelone J. P., Morgan V. I., Boutron C. F. and Rosman K. J. R. (2008) The lead pollution history of Law Dome, Antarctica, from isotopic measurements on ice cores. *Earth Planet. Sci. Lett.* **204**, 291–306.
- Vanderstraeten P., Lénelle Y., Meurrens A., Carati D., Brenig L., Delcloo A., Offer Z. Y. and Zaady E. (2008) Dust storm originate from Sahara covering Western Europe: a case study. *Atmos. Environ.* **42**, 5489–5493.
- Verniers J., Herbosch A., Vanguetaine M., Geukens F., Delcambre B., Pingot J. L., Belanger I., Hennebert M., Debacker T. N., Sintubin M. and De Vos W. (2001) Cambrian-Ordovician-Silurian lithostratigraphic units (Belgium). *Geol. Belg.* **4**, 5–38.
- Vouk V. B. and Piver W. T. (1983) Metallic elements in fossil fuel combustion products: Amounts and form of emissions and evaluation of carcinogenicity and mutagenicity. *Environ. Health Perspect.* **47**, 201–225.
- Wardenaar E. (1987) A new hand tool for cutting peat profiles. *Rev. Can. Botan.* **65**, 1771–1772.
- Wasserburg G. J., Jacobsen S. B., De Paolo D. J., McCulloch M. T. and Wen T. (1981) Precise determination of Sm/Nd ratios, Sm and Nd isotopic abundances in standard solutions. *Geochim. Cosmochim. Acta* **45**, 2311–2323.
- Wastiaux C. and Schumacker R. (2003) Topographie de surface et de subsurface des zones tourbeuses des réserves naturelles domaniales des Hautes-Fagnes. Convention C60 entre le Ministère de la Région Wallonne, Direction générale des Ressources naturelles et de l'Environnement, et l'Université de Liège. Unpublished report, 52 p. + annexes. In French.
- White J. R., Cerveny R. S. and Baling R. C. (2012) Seasonality in European red dust/blood rain events. *Am. Meteor. Soc. BAMS* **471–476**. <http://dx.doi.org/10.1175/BAMS-D-11-00141.1>.
- Yliruokanen I. and Lehto S. (1995) The occurrence of rare earth elements in some finnish mires. *Bull. Geol. Soc. Finland*, 27–38.